ANALYSIS OF ELASTIC-PLASTIC INTERFERENCE FIT JOINTS

A MASTER'S THESIS

in

Manufacturing Engineering

Atılım University

by

H. Hava Işık

OCTOBER 2015

ANALYSIS OF ELASTIC-PLASTIC INTERFERENCE FIT JOINTS

A THESIS SUBMITTED TO

THE GRADUATE SCHOOL OF NATURAL AND APPLIED SCIENCES

OF

ATILIM UNIVERSITY

BY

H. HAVA IŞIK

IN PARTIAL FULFILLMENT OF THE REQUIREMENTS FOR THE DEGREE OF

MASTER OF SCIENCE

IN

THE DEPARTMENT OF MANUFACTURING ENGINEERING

OCTOBER 2015

Approval of the Graduate School of Natural and Applied Sciences, Atılım University.

_____

Prof. Dr. İbrahim Akman

Director

I certify that this thesis satisfies all the requirements as a thesis for the degree of Master of Science.

_____

Prof. Dr. Engin S. Kılıç

Head of Department

This is to certify that we have read the thesis "Analysis of Elastic-Plastic Interference Fit Joints" submitted by "H. Hava IŞIK" and that in our opinion it is fully adequate, in scope and quality, as a thesis for the degree of Master of Science.

Asst. Prof. Dr. Celalettin Karadoğan
Co-Supervisor

Asst. Prof. Dr. Omer Music
Supervisor

Examining Committee Members

Asst. Prof. Dr. Mert Efe _____

Asst. Prof. Omer Music _____

Asst. Prof. Dr. Celalettin Karadoğan _____

Asst. Prof. Dr. Kemal Davut _____

Asst. Prof. Dr. Caner Şimşir _____

Date: 20.10.2015

I declare and guarantee that all data, knowledge and information in this document has been obtained, processed and presented in accordance with academic rules and ethical conduct. Based on these rules and conduct, I have fully cited and referenced all material and results that are not original to this work.

H. Hava Işık

ABSTRACT

ANALYSIS OF ELASTIC-PLASTIC INTERFERENCE FIT JOINTS

Işık, H. Hava

M.S., Manufacturing Engineering Department

Supervisor: Asst. Prof. Dr. Omer Music

Co-Supervisor: Asst. Prof. Dr. Celalettin Karadoğan

October 2015, 66 pages

In automotive industry, increasing product complexity has driven the development of new joining processes for mechanical parts. Typical examples are welding, adhesive bonding and mechanical fastening used to join components in a product assembly. Joining by interference fits belongs to a wider group of mechanical joining processes, some examples of which are self-pierce rivets, mechanical clinches, pin joints and threaded connections.

In interference-fit joints, interference of two mating parts leads to contact pressure at the interface. This contact pressure holds the two parts together through friction, providing a mechanical joint. Strength of this joint depends mainly on the coefficient of friction, contact pressure and contact area. Such joints are used in a wide variety of applications, ranging from automobile to aerospace industry.

This study focuses on analysis of elastic-plastic interference fit joints formed by fitting the filter pin into the cylindrical hole in the injector body. This process has been studied in detail, however a review of literature reveals that analytical and numerical models have been developed for relatively simple geometries, and the number of publications for complex, asymmetric, three-dimensional geometries is limited.

This study presents a detailed examination of the elastic-plastic interference fit joints for both simple and complex geometries. The mechanics of the process is studied in detail through physical trials, analytical and numerical models. Both trials and modelling are done for two-dimensional and three-dimensional geometries. The effects of geometrical properties, material properties and cylinder-tube, grooved geometry and actual process are investigated.

Developed numerical models are applied to an industrial problem; analysis of an asymmetric, three-dimensional interference fit joints used in high pressure diesel injection systems, specifically the joint between the fuel filter and the injector body of an injection system. Strength of this joint is one of the key parameters determining the performance of the fuel injection system as a whole and as such is studied in detail. A detailed investigation of the joining process shows that the joint strength can be improved through careful selection of filter and body materials, geometry and other parameters that affect the joining process.

Keywords: Interference fit, Elastic-plastic, Joining

ÖZ

ELASTİK-PLASTİK SIKI GEÇME PROSESİNİN İNCELENMESİ

H.Hava, Işık

Yüksek Lisans, İmalat Mühendisliği Bölümü

Tez Yöneticisi: Yrd. Doç. Dr. Omer Music

Ortak Tez Yöneticisi: Yrd. Doç. Dr. Celalettin Karadoğan

Ekim 2015, 66 sayfa

Başta otomotiv ve uçak sanayisinde olmak üzere tasarlanan ürünlerin karmaşıklığı arttıkça mekanik parçaların montajlanması için yeni prosesler geliştirilmektedir. Sıkı geçme prosesi bu yöntemlerden bir tanesidir. Sıkı geçme prosesi, iki farklı geometrideki parçanın birbirine arayüzeyinde oluşacak olan temas basıncı ile tutunarak mekanik bir geçme sağlamaktadır. Geçme dayanımı genel olarak, temas alanı, arayüzey basıncı ve sürtünmeye bağlı olarak değişmektedir.

Bu çalışma, silindirik bir tüp içerisine pimin çakılması ile oluşan elastik- plastik sıkı geçme analizlerini ele almaktadır. Literatür araştırması yapıldığında elastik-plastik geçme için analitik modelin bulunmaması ve sayısal modellerde ise basit geometri kullanılarak araştırmaların tamamlandığı gözlemlenmiştir. Yapılan çalışma ile birlikte analitik model oluşturularak, enjeksiyon sistemlerinde bulunan filtre gibi karmaşık bir geometri üzerinde sayısal modelleme oluşturulması planlanmıştır.

Yüksek basınçlı dizel enjeksiyon sistemlerinde bullunan ve sıkı geçme yöntemi ile enjektöre çakma işlemi ile birleştirilen yakıt filtresi, dizel enjeksiyon sisteminin performansını etkileyen ve sınırlayan önemli unsurlardan bir tanesidir. Sıkı geçme prosesine etki edebilecek olan parametrelerin araştırılması tezin amaçlarından bir tanesidir. Bu çalışmada oluşturulan parametre çalışmaları ile, basit geometriden karmaşık geometriye kadar, deneysel, nümerik ve analitik çözümler kullanılarak sistem ve proses mekaniğine olan etkilerinin incelenmesi amaçlanmıştır.

Anahtar Kelimeler : Sıkı geçme, elastik-plastik, birleştirme

To My Family

ACKNOWLEDGEMENT

I would like to express my special thanks to my supervisor Asst. Prof. Dr. Omer Music for his suggestions, encouragement, guidance and invaluable help. I would like to my co-supervisor Asst. Prof. Dr. Celalettin Karadoğan for his guidance, and support.

I also would like to thank Asst. Prof. Dr. İzzet Özdemir, Asst. Prof. Dr. Caner Şimşir, and Asst. Prof. Dr. Kemal Davut who taught me during my undergraduate and graduate studies. I have performed all my studies at the Metal Forming Centre of Excellence (MFCE), and would like to thank Prof. Dr. Bilgin Kaftanoğlu and members of the MFCE.

Most of the materials and items used in thesis are provided by Bosch Sanayi ve Ticaret A.Ş. I am very grateful to Section Manager of the Research and Development Department of Bosch, Çağdaş Bayram and Development Engineer Ms. Asuman Koç. This study was conducted as part of an industrial research project supported by TÜBİTAK (The Scientific and Technological Research Council of Turkey), grant number 3120409.

Special thanks to Ebru Arslan, Oğuzhan Herkiloğlu for their precious help and support which made the achievement of this thesis possible. I also would like to thank to Zeynep Öztürk for her kind help.

I would like to express my special appreciation and happiness to my husband Eren Işık for his priceless support, encouragement and endless love.

Finally, I would like to express gratitude to my parents and brother; Ceylan, Nezahat and Osman Hüyük for their endless support, encouragement and priceless help during my thesis work.

TABLE OF CONTENTS

LIST OF TABLES

LIST OF FIGURES

LIST OF ABREVIATIONS

ECM	Engine Control Module
CRI	Common Rail Injector
FEM	Finite Element Method
FEA	Finite Element Analysis
MFCE	Metal Forming Center of Excellence
FM	Friction Model
3D	Three Dimensional
2D	Two Dimensional
Mn	Manganese
Pb	Lead
K	Potassium
S	Sulphur

NOMENCLATURE

F	Axial force
Δh	Change in height
A	Instantaneous cross-sectional area
ε	True strain
C	Stress Coefficient
τ	Friction Stress
f	Friction Factor
α	Ratio of real contact to the apparent contact area
σ_0	Flow stress
τ/k	Dimensionless friction stress
p/σ_0	Dimensionless normal pressure
τ^*	Friction stress
p^*	Normal pressure
D_{iA}	Inner diameter of the outer part
D_{aA}	Outer diameter of the outer part
D_{aL}	Outer diameter of the inner part
D_{iL}	Inner diameter of the inner part
L_f	Length of the joint
U_i	Actual interference
D_f	Diameter of the joint
U_w	Effective interference

CHAPTER 1

INTRODUCTION

In automotive industry, increasing product quality has driven the development of new joining process for mechanical parts. To assemble mechanical parts, many new processes have been developed. Joining by interference fits belongs to wider group of such mechanical fastening and joining processes, examples of which are pin joints, threaded connections, rivets and gaskets. Such mechanical fastening and joining methods are used in assembly for their mechanical strength, reliability, reusability and appearance.

Common rail injection system is a modern variant of direct fuel injection system for petrol and diesel engines. On diesel engines, the common rail injection system feeds individual solenoid valves with high pressure fuel (over 1000 bars), as opposed to low pressure fuel pump feeding unit injectors.

Piezoelectric valves make possible fine electronic control over the fuel injection time and quantity, and the higher pressure that the common rail technology provides better fuel atomization [1].

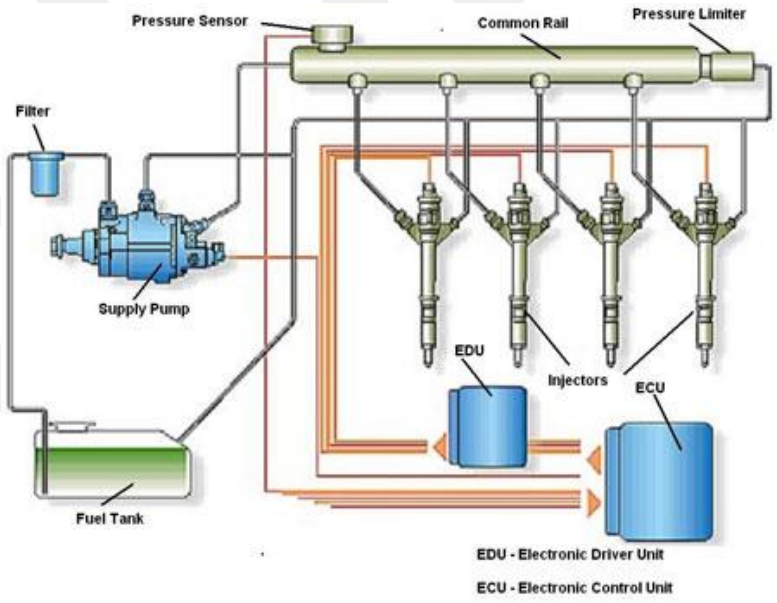

Figure 1.1 Diagram of common rail system

The term ‘common rail’ refers to fact that all of the fuel injectors are supplied by a common fuel rail which is nothing more than a pressure accumulator where the fuel

is stored at high pressure. Figure 1.1 represents the common rail system and its components. This accumulator supplies multiple fuel injectors with high pressure fuel. This simplifies the purpose of the high pressure pump in that it only needs to maintain a commanded pressure at target.

Fuel injector system basically injects a specific amount of fuel in the combustion chamber of an internal combustion engine according to the requirements of the engine. Initially, carburetors were used as an input of fuel supply to the gasoline engines before the use of fuel injection systems. Fuel injector is a valve that is controlled by the ECM (Engine Control Module). The injectors according to the load on the engine are able to open a number of times in the matter of few seconds. Following are some of the types of Fuel Injector systems used in cars;

- Carburetor
- Throttle Body Injection
- Multi Point Fuel Injection
- Common rail direct injection

1.1 Problem Definition

In common rail systems, when the fuel injectors are electrically activated; a hydraulic valve is mechanically or hydraulically opened and fuel is sprayed into the cylinders at the desired pressure [1].

Fuel injectors have many critical components for balancing fuel pressure, preventing particle and the other missions. Following are injector components;

- Injector Body
- Actuator Module
- Coupler Module
- Nozzle Module
- Fuel Filter

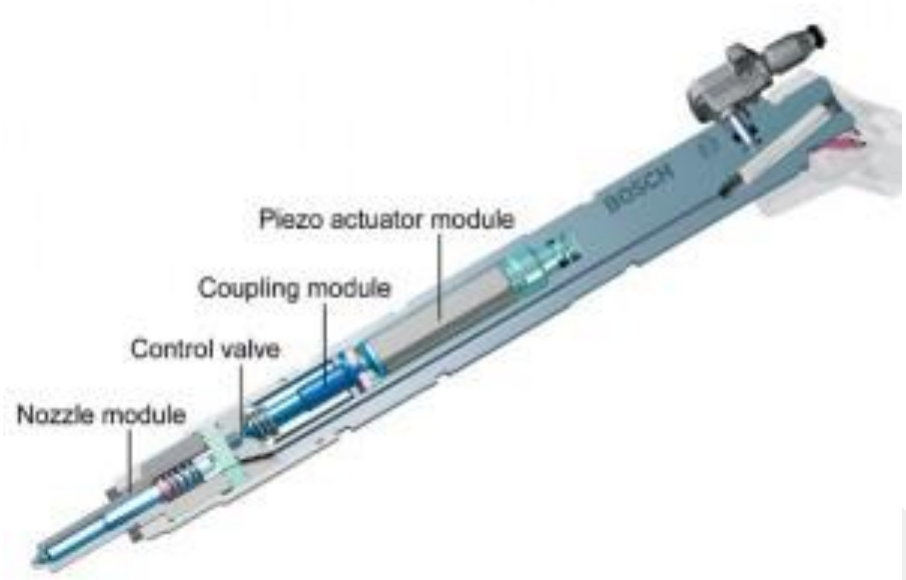

Figure 1.2 Fuel Injection System Components

Fuel injection system components are shown in Figure 1.2. As illustrated in this figure, the injection system is designed by BOSCH and is named CRI-3 (Common Rail Injectors, 3rd generation which is resistant up to 2000 bars). The most critical part of the injector is fuel filter. Fuel filter is a filter in the fuel line that screens out dirt and rust particles from the fuel. Fuel filters serve vital function, unfiltered fuel may contain several kinds of contamination, if substances are not removed before the fuel enters the system, and they will cause rapid wear and failure of the injectors due to the abrasive action of the particles on the high precision components used in injection systems.

To assemble the injector and fuel filter, interference fit joint method is used. In assembly part, system has been affected by numerous parameters. The grooved filter has been used for high pressure injection systems. These grooves provide entering fuel into the system and also avoid unwanted and big particles. To investigate parameters which affect to the joining process and make process more understandable, this study has been done.

Injector and position of the filter are schematically shown in Figure 1.3. In interference fit joints, difference in geometry of two mating parts leads to contact pressure of the interface.

This contact pressure holds the two parts together through friction, creating a mechanical joint [2]. This study begins with literature survey of the interference fit joining, material characterization of filter and injector body and boundary conditions of the process. It's followed by numerical, analytical and experimental researches of the joining process and, lastly, a set of conclusions is drawn from the results of the physical trials and numerical analysis. Also, numerous parameters that can affect to the process are investigated by using experimental and numerical methods. This study focuses on interference fit joints for simple pin- body and complex shape of the injection system.

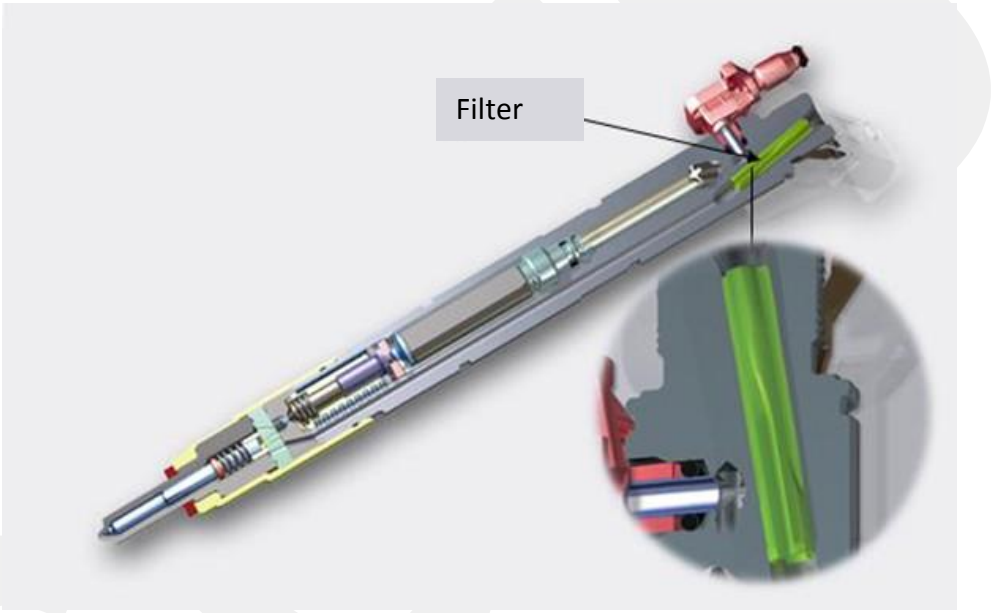

Figure 1.3 Injector - Filter Location

The aim of this study is to investigate parameters of joining process and effects on pin design. The literature survey reveals that, analytical and numerical models for joining process have been developed for relatively simple geometries and consequently numbers of publications for complex, asymmetric, three dimensional geometries is limited. One of the scope of this study is to make contributions to understandability of this process.

Next chapter of this study is the review of literature about joining processes.

CHAPTER 2

LITERATURE SURVEY

2.1 Introduction

Joining by interference fits refers to joining of two (typically) cylindrical components, a pin and a body. The fit is formed by pressing or shrinking the pin into a body, which creates a contact pressure and most importantly, a friction force at the interface between the two mating components. This type of joining is typically used where a transmission of both an axial force and a torque is required.

The review starts by classifying and describing the interference fits and its various configurations. This is followed by a description of the process in detail. Next, a summary of numerical, analytical and experimental techniques are reviewed and discussed, grouped into numerical, analytical and experimental categories. Finally, recent developments are reviewed and discussed in detail.

2.2 Features and Classification

Joining by interference fits (fitting) belongs to a wider group of mechanical fastening and joining processes. Interference in an interference fitted assembly provides contact pressure between the mating components. Such joints have an excellent load bearing ability under both static and dynamic loading conditions. This makes them attractive for a wide range of engineering applications; bearing body, pump impellers fitted on shafts, valve seats, gear-shaft joints and joints on mechanical drives.

The only classification of fits appears to be the classification based on the amount of interference between the pin and the body. Depending on the dimensions of the pin and the body, the fits are classified into clearance fits, transition fits and interference fits. The clearance fit allows for a relative motion between the mating parts, while the interference fit provides a tight joint between the two mating parts.

2.3 Terminology

The terms used for interference fits in industry and academic literature vary and generally not accepted vocabulary has been established. The terms used in this review

are summarized in Table 2.1, along with a list of alternatives as used variously in academic publications and industry.

Table 2.1 Terminology

Term		***Alternatives***	***Explanation***
Turkish	*English*		
Sıkı Geçme	Interference fit	Shrink-fit, press-fit, end-fit	Joint between two parts is achieved by friction after the parts are pushed together.
Sıkı Geçme (Sıcak)	Shrink fit		fit created by heating or cooling the components and before pushing the pin into a body.
Baskılı Geçme	Press fit	Drive fit	fit created by body the pin into a body.
Sıkı Geçme ile Birleştirme	Joining by an interference fit	Fitting, interference joint, interference fitting, shrink-fitted joint	Self-explanatory.
Pim	Pin	Shaft	Male part of the assembly.
Gövde (Pim Yuvası)	Body	Body, bush, hub	Female part of the assembly. Any component that is fitted on the pin.
Temas Yüzeyi Gerilimi	Contact stress	Interface stress	The stress induced at the interface between the pin and the body.
Geçme Toleransı	Interference	Deformation	The amount of overlap between the pin and the body.
Yağlayıcı olmadan Yapılan (Kuru) Geçme	Dry-fit	Non-lubricated fit	A fit applied without a lubricant.

2.4 Process Description

The performance of the pin and body assembly depends on the type of fit between the mating parts. By varying the sizes of two mating parts, numerous types of fits can be obtained. Depending upon the actual limits of the hole and shaft the fits are classified into clearance fits, transition fits and interference fits. The clearance fit provides a relative motion between the pin and the body. While the transition fit can produce either a clearance fit or an interference fit, the interference fit creates a tight joint between the pin and the body.

Interference connections are widely used in practice for transmission of torque, axial forces, and bending moments. Connections between the two components are spread along the cylindrical surfaces of the two mating parts. The nature of joint is such that the shaft is connected to a body with a hole diameter slightly smaller than that of the shaft. Strain at the interface of the two parts gives rise to contact pressure 'p'. This pressure produces a frictional force on the interface that allows the components to carry an external axial force and torque.

Joints produce by interference fits are divided into three, depending on the installation method; first, joints obtained by heating the body and inserting the pin, second, joints produced by cooling the pin and third, joints produced by pushing the pin into the body while both are at room temperature. Installation is carried out on hydraulic, screw, or lever presses. To prevent damage to the surface and to decrease the installation forces the mating surfaces are generally lubricated with oil. It should be noted that in case of heating, the temperature must be lower than that of low-temperature tempering, to avoid structural changes in the metal.

2.5 Analysis of joining by interference fits

Analysis of interference fit joints has been developed by systematic investigations of the process using analytical, numerical and experimental techniques. This section presents a survey of the analysis techniques published in academic literature.

2.5.1 Experimental

In studies of interference fits, experimental techniques have been applied to investigate the contact pressure and its distribution, the strength of the joint, the effect of bonding agents and the effect of surface properties.

To estimate the contact pressure in interference fits, both Croccolo et al (2011) and Kim and Lee (2006) measured the circumferential strain on the bushing by applying a strain gauge to the outer diameter of the bushing (Figure 2.1 below), which then allowed them to estimate the contact pressure through analytical equations [3], [4]. In a more recent study, Croccolo et al (2012) used this analytical model to determine the friction coefficient in interference fits between aluminum and steel [5]. This was done by measuring the push-out force of an interference fit while estimating the contact pressure from the strain measurements. They show that the friction coefficient for dry press-fitted aluminum-steel joints is 0.46.

Figure 2.1 Example of strain gauge application on the external surface of the body (quarter-bridge connection in a Wheatstone circuit by Croccolo, 2011).

Another method for measuring contact (interface) pressure and its distribution in interference fits was developed by Lewis et al (2005) by using ultrasound measurements. Their measurements show a central region of uniform pressure with higher pressure at the edges. The magnitude of the uniform pressure agrees well will Lamé analysis. They compare the contact pressure distributions in shrink and press fits, and show that the pressure is more uniform in case of press fits, suggesting that this is due to plastic deformation of the surfaces as they slide against each other [6].

2.5.2 Analytical

Theoretical techniques can provide insights into the detailed evolution and stresses and strains throughout the parts and during the fitting process. This information can then be applied to understand the mechanics of the process and predict the strength of the joint.

Most of the analytical models used to design interference fits are based on the equations established by Lamé (Shigley and Mischke, 1988), which are based on a two-dimensional stress analysis in the elastic range. However, Lamé's solution is limited by its simplifying assumptions. This approach will not predict the stress concentrations at the ends of the joint and it is not suitable for a bushing with varying cross-section (conical interference fit).

The analytical models have been used to investigate the contact pressure and stress distribution in interference fits, the effect of surface roughness and thermal cycles and to study bonded (glued) fits.

Kawamura et al (2003) developed an analytical model for interference fits with anaerobic adhesives. The model uses theory of elasticity to estimate the contact pressure and models the bushing, the pin as well as the adhesive as a separate cylinder of a given shear strength. They show that the model estimates the joint strength well for adhesive joints, but severely overestimates the dry joints [7].

Yang et al (2001) studied the influence of surface roughness on cylindrical shrink fits. They point out the importance of surface roughness in interference fit and demonstrate experimentally that a major factor affecting the fit strength is the mean height of the surface asperities; the extraction load varies by up to 300% for R_a values of 0.24-6.82 μm [8].

Zhang et al (2000) analyzed an interference fit of a ring gear and a stepped shaft using both numerical and analytical methods and conclude that the Lame's equations underestimate the change in diameter and therefore both circumferential and radial (contact) pressure by up to 78%. This is mainly due to the relatively complex geometry of the mating parts [9].

To estimate the contact pressure, Croccolo et al (2011) measured the circumferential strain on the bushing through a strain gauge at the outer diameter of the bushing. Using thick-walled cylinder theory, this strain was then used to estimate the contact pressure [4].

To estimate contact pressure between two different materials (different Young's moduli), Croccolo et al (2012) reports on an analytical model which accounts for difference in stiffness of the mating materials. The authors also point out that if the

stiffnesses of the two parts are close, the actual interference is likely to be less than the estimated interference, due to surface roughness effects.

Lippmann (1992) used an analytical model to study the effect of thermal cycles on cylindrical fits. The author concludes that the contact pressure changes with temperature. Perhaps more importantly, the increase in temperature leads to a decrease in yield stress and may cause plastic deformation in the fit, causing a drop in contact pressure at the end of the cycle, therefore reducing the load capacity of the fit [10].

Eyercioglu et al (2009) compared analytical and numerical solutions for shrink fits used for dies in precision forging and report that the Lamé solution underestimates fitting stresses concluding that numerical methods are a must for accurate prediction of stresses in fits [11].

Yoneno et al (1997) analyzed strength of bonded (glued) shrink-fitted joints under axial loads using theory of elasticity. The adhesive layer is modelled as a hollow cylinder, so that the problem is modelled as a contact problem using axisymmetric theory of elasticity. This allows for a detailed calculation of the stress distribution at the interfaces and an estimate of the joint strength. Comparison with experiments shows that the analytical model is accurate to within ~15% [12].

One of the analytical analyses is specification of DIN standard. This standard specifies the basis of the calculation for the interference fits with cylindrical effective surfaces, the parts of which consist of metallic materials. This study consists of calculation of interference fits, coefficients of adhesion of interference fits, design and assembly of interference fits and instructions for manufacturing. To create an analytical model for joining process, this study and information are used. Basic principle of these studies is applicable to the interference fits with same constant axial length for inner and outer parts. Detailed information will be given 'analytical solution' section.

2.5.3 Numerical

Experimental and analytical techniques as presented in the previous sections are useful tools allowing for prediction of a number of parameters affecting the process. However, for a more detailed analysis of the process, numerical methods are required. These methods can ideally enable detailed prediction of all the parameters related to

the process, thus enabling prediction of joint quality, the design of the fitting process and an examination of the joint behavior in service.

Zhang et al (2000) used ANSYS software package to analyses interference fits of ring gears on wheels, using an elastic two-dimensional model with coulomb friction. Their results show stress concentrations close to the edges, as also measured by Lewis et al (2005). They also suggest selective assembly approach, which reduces variations in interference and therefore increases reliability of the interference fit joints. Eyercioglu et al (2009) followed a very similar approach using an elastic two-dimensional model in ANSYS with Coulomb friction and numerical parameters to model shrink fits in precision forging dies. However, there is no validation of the numerical experiments in both papers, suggesting that the results are more qualitative than quantitative and as such useful for studying trends only. It is worth mentioning that both studies used a coefficient of friction of 0.2.

Wang et al (1994) compared the performance of lugs under various clearance and interference values and concludes that using a carefully adjusted interference fit increases the durability of the joint [13].

Yang et al (2001) used an elastic two-dimensional model developed in D'assault Systèmes Abaqus software package to study the effect of surface roughness on shrink fits [8]. They modeled the surface asperities on both the pin and the bushing, and point out that to model the fit accurately, it is necessary to have a node at every peak and valley. Their model is compared to experiments, and shows a maximum difference of 9%, which is likely to have occurred due to numerical errors, inaccuracies in experimental data and simplified friction model. Perhaps more importantly, their analysis suggests that the in spite of high stresses tending to crush the asperities, they tend to persist even under high pressures.

Chakherlou et al (2009, 2010) and Kiral (2009) used ANSYS to develop elastic-plastic three-dimensional models of lap joints and pin joints, and used it to study the effect of interference fit on fatigue life [14], [15]. They show that the interference fit in such joints increases joint strength and reduces the stress amplitude, resulting in increased fatigue life. However, Chakherlou et al (2010) report out that beyond certain interference, there is no increase in fatigue life.

Bernd-Ardo et al (2011) examine advance friction modeling for bulk metal forming process. In order to obtain high accuracy in simulation results, exact knowledge of process condition is required. Due to the fact that, friction in the contact area has a significant impact on the material flow during the forming process. The most influencing factors are contact pressure, roughness, sliding velocity and flow behavior of the material. Also constant friction model does not represent the state of art tribology. They develop a new friction model taking into account the sliding velocity between tool and the work piece, and it is implemented in commercial FE software. The process simulations showed that using the new friction model leads to more accurate prediction of the geometry, as well as the forming process [16].

Xincai Tan compare friction models in the bulk metal forming. The friction model is important to control the accuracy of necessary output results predicted [17]. The various friction models, which are Coulomb Friction Model, the constant friction model, the general friction model, the absolute constant and empirical friction model to perform of upsetting AA6082 lubricated with four lubricants are used. It's concluded that; the calibration curves of the friction area ratio are more sensitive to friction at the tool/work piece interface than those of normal pressure. The normal pressure curves from FEM predictions are higher than those experiments, for all of the chosen friction models, under fitness of friction area ratio curves theoretically predicted to those experimentally measured.

Petersen et al (1995) investigate friction in bulk metal forming. In this study, the application of the general friction model, developed by Wanheim and Bay, involves a major improvement in the ability to simulate processes where low tool-work piece interface stresses may prevail. This is confirmed by experimental and numerical investigations into the upsetting of a semi-tapered specimen between parallel dies. Also it has led to proposal of a new ring compression test geometry intended to complement the conventional ring test for the calibration of friction models under conditions where the normal stresses over considerable parts of the tool-work piece interface may be lower than the yield stress of the material [18].

One of the Wanheim’s study, Amonton's law gives occasion for an overestimation of the friction stresses at the tool- work piece interface, because the normal pressure often is considerably greater than the yield stress of material: consequently, the friction

stress becomes greater than the yield stress of the material in pure shear. Wanheim, Bay developed a new general friction model for expressing friction at the tool-work piece interface [19].

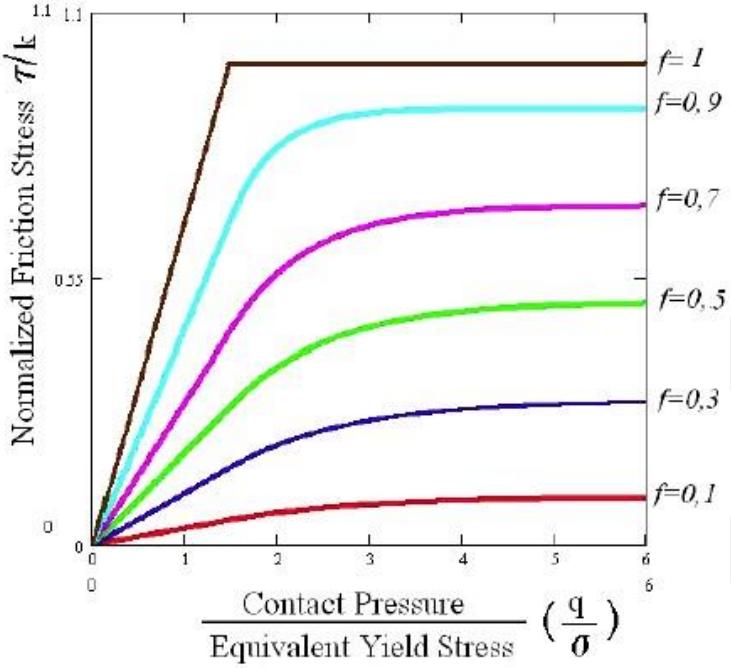

Figure 2.2 Normalized friction stress as a function of nominal normal pressure and friction factor [19]

As shown in the figure, the model assumes to be proportional to the normal stress at low normal pressure, but going towards a constant value at high normal pressure and two section being combined with a transition region. However, this model is limited to small deformation stages of deformation. Detailed information and calculations will be given in the following sections.

2.6 Recent developments

The recent development have reported in literature have focused on increasing the joint strength and developing methods to investigate the contact pressure in the process.

Cao and Qin (2011) proposed and investigated the process of interference fitting using the stress wave method. In this method, a force is applied to the pin for a very short period of time. This produces an elastic stress wave in the pin, which results in tension along the axis of the pin and due to Poisson effect, a reduction in diameter. This reduction allows for an easy and quick installation of the pin in the bushing. The

main advantage of this method is that it allows higher interference values compared to the conventional methods. At high interference values, conventional methods, where the pin is pushed into the bushing using either a pneumatic or a hydraulic force, are likely to cause damage to the joint and are therefore limited. The stress wave method claims to overcome this limitation.

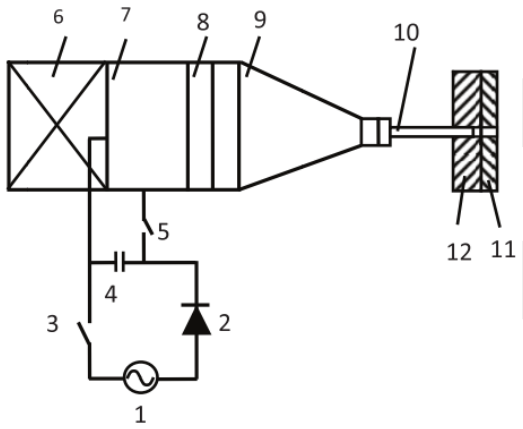

Figure 2.3 Schematic representation of the stress wave device: 1 power supply 2 Rectifier 3 recharge switch 4 capacitor bank (Cao and Qin 2011).

Ramamoorthy and Radhakrishnan (1992) proposed surface strengthening by roller burnishing to improve fatigue and corrosion strength through compressive residual stress and to obtain a uniform finish of surfaces in interference fits. Their results indicate that when the pin is ground, roller burnished, assembled and then strain-aged at a high temperature (300-500 °C), the load capacity of the joint increases by up to 5 times.

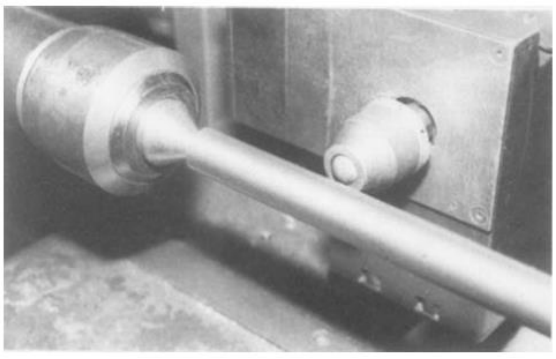

Figure 2.4 Roller burnishing setup showing the burnishing tool and the workpiece Roller burnishing setup showing the burnishing tool and the workpiece (Ramamoorthy and Radhakrishnan, 1992).

To improve load carrying capacity of conical interference fit joints in torsion, Sniezek et al (2010) proposed creating interlocking laser-hardened zones on both the pin and the bushing, shown in the figure below. Following a detailed numerical analysis and experimental validation, they concluded that this approach increases the torsional capacity of the joint by up to 50%.

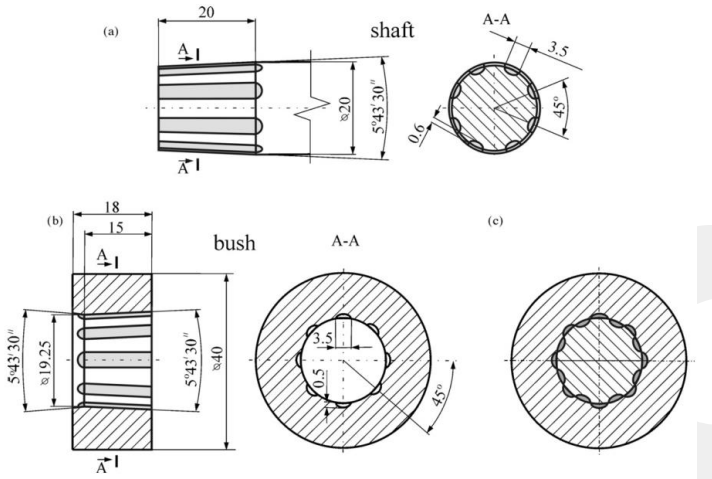

Figure 2.5 Geometry (linear dimensions [mm]) of elements of the conical interference-fit joint with laser reinforcement zones Sniezek et al (2010).

Lewis et al (2005) developed a method for measuring contact (interface) pressure in interference fit using ultrasound measurements and applied it successfully to study contact pressure and its distribution in interference fits.

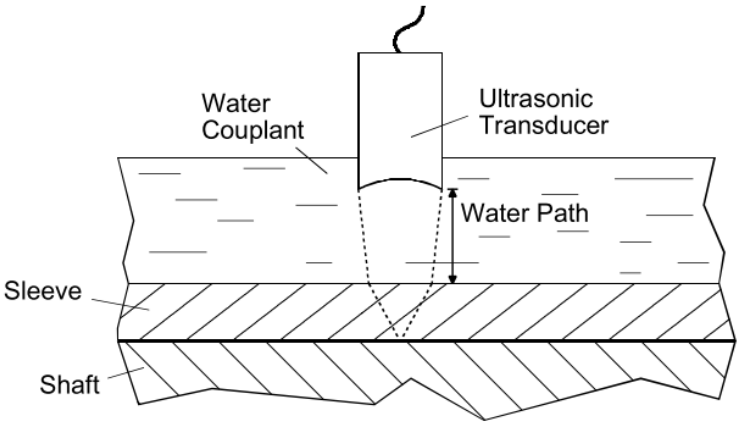

Figure 2.6 Contact pressure measurement using ultrasound

Yoneno et al (1997) analyzed strength of bonded (glued) shrink-fitted joints under axial loads using theory of elasticity and a set of experiments. Their model suggests that the strength of a bonded joint depends on the ratio of outer diameter of bushing to

the pin and the pin-bushing contact length. Perhaps more importantly, in a comparison of shrink-fitted and glued-shrink-fitted joints, they show that the strength of bonded joints is independent of the amount of interference. Their final conclusion is that the glued joints are clearly superior to conventional non-adhesive joints.

2.7 Conclusion

The review has revealed several gaps in current knowledge of mechanics of interference fits. Studies of recent developments in joining by interference fits have shown that great potential for innovation exists. This review aims to fill this need in order to identify gaps in existing knowledge and to enable transfer of knowledge to future studies.

CHAPTER 3

MATERIAL CHARACTERIZATION AND DETERMINATION OF BOUNDARY CONDITIONS

3.1. Material Characterization

Material characterization is essential for finite element analysis (FEA) as the accuracy of the outputs of the simulation depends on the quality of the input material data. Tension and compression testing are two of the most basic and most useful types of testing for obtaining material properties. Typical analytical information derived from tension and compression testing includes the following: compressive strength, elastic limit, elongation, reduction in area, strain, yield point, yield strength and ultimate tensile strength. In this study, 11SMnPb30 and C45PbK steels are used for material characterization. These steels are two different types of widely available non-alloyed free machining steels, representative of steels used in interference fit joints.

3.1.1 Simple Compression Test

Simple compression test has been done to determine the flow curves of the interference fit process materials which are pin (11SMnPb30) and tube (C45PbK) steels. The following sub-parts provide a detailed description of the test setup, test procedure and the equations used to evaluate the test data.

In the compression test, a cylindrical test specimen is compressed along its axis while recording the axial load and the change in specimen height. The true (flow) stress σ_0 and the total true strain φ, are calculated from the axial load (F) and the change in height (Δh) using equations Eq.3.1 and Eq.3.2.

$$k_f = \frac{F}{A} \qquad \text{Eq. 3.1}$$

$$\varepsilon = \ln\left(\frac{h}{h_0}\right) = \ln\frac{h_0+\Delta h}{h_0} \qquad \text{Eq. 3.2}$$

The true area (A- instantaneous cross- sectional area) required for the calculation of the true stress is calculated from volume constancy using Eq.4.3;

$$A = \frac{V}{l} = \frac{h_0 * A_0}{h_0 + \Delta h} \qquad \text{Eq. 3.3}$$

Test setup and procedure:

The compression tests were performed in Metal Forming Center of Excellence (MFCE) using Zwick/Roell Z300 tensile testing device with 300 kN capacity (Figure 3.1). Cylindrical specimens of d_0 =12 mm, l_0 =24 mm (tube) and d_0 =4 mm, l_0 =8 mm (pin) were tested at room temperature. Test specimens compressed to approximately half of the initial length.

Procedure followed in the tests is as follow;

- Measuring the specimens
- Apply the lubricant
- Apply a preload of 100 N
- At constant speed, deform the specimen to the half of the initial length
- Measure the specimen dimensions at the end of the test

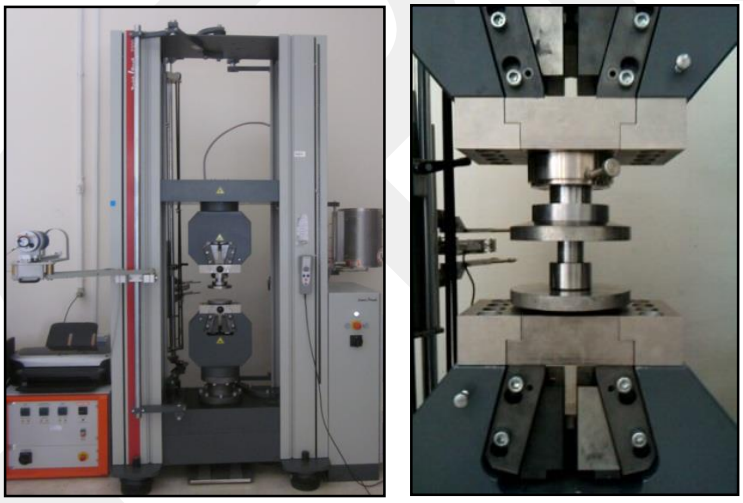

Figure 3.1 (a) Compression test setup at MFCE and (b) the compression test is being performed by using compression apparatus.

The flow curves obtained from the compression test have been evaluated up to the strain value 0.5, but in typical metal forming process, this value may reach a value of up to 3. Therefore, flow curves were extrapolated by using Ludwik-Hollomon equation.

Ludwik-Hollomon equation is given below;

$$k_f = C * \varepsilon^n \qquad Eq. 3.4$$

Where, C is stress coefficient (material constant), ε is the true strain and n is the strain hardening coefficient. Curve fitting for analytical model is done by using least squares method. Calculated constants are shown in Table 3.1 for pin and tube material.

Table 3.1 Calculated constants by using Ludwik-Hollomon equation

	Tube	**Pin**
C (MPa):	1202	923.7
n (-):	0.093	0.029

Compression test and extrapolated curves are shown in Figure 3.2. Maximum difference between analytical (extrapolated) and experimental curves is less than 4%.

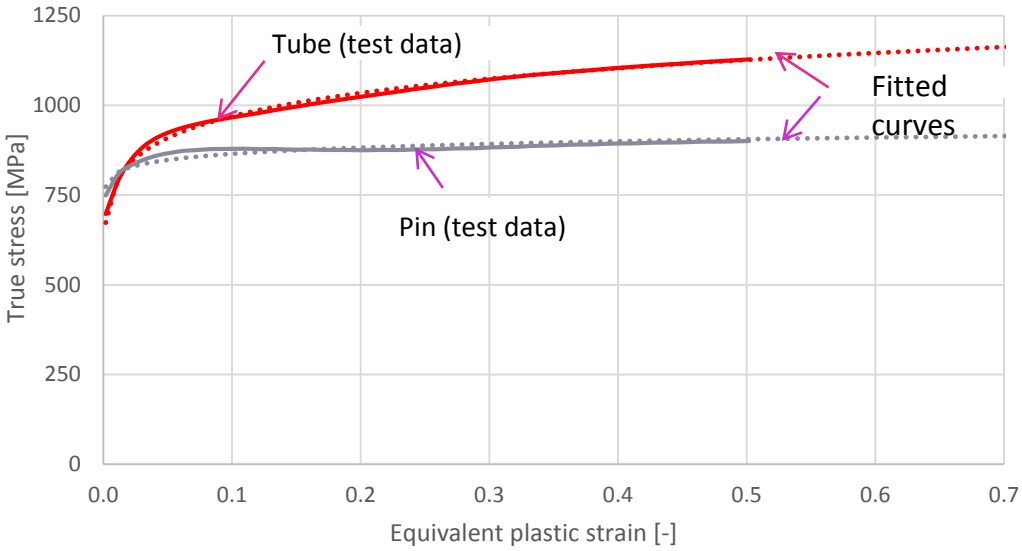

Figure 3.2 Analytical and Experimental Flow Curves of Pin and Tube

According to results, there is a significant difference between pin and tube's flow curves. Both of them start to yield at the same value but the work hardening behaviors are different from each other. As tube hardens quickly, the pin almost never hardens. In other words, pin undergoes plastic deformation mainly.

3.1.2 Uniaxial Tensile Test

Uniaxial tensile test is one of the most commonly used test for evaluating material properties. This test is preferable due to its simplicity and well defined testing standards. In the simplest form, the tension test is accomplished by gripping from opposite ends of a test item within the load frame of a test machine.

Like compression test, Zwick Roell 300kN tension compression machine is used for tensile test. Tensile test is carried out by extension of circular specimen (Figure 3.3) with two jaws. One of the jaw is fixed and the other can be moved in other direction by applying force. Circular test specimen, which is shown in Figure 3.3, is pulled till the breaking point, at the same time, load (P) and extension (Δl) is recorded by test machine.

Figure 3.3 Tensile Test Circular Specimen (End of the test)

After the tests, the force-displacement datum is converted into stress-strain curves using the true stress and true strain expressions. These equations are valid till necking point. All the equations are given in the 'Simple Compression Test' subsection.

Test setup and procedure:

Like compression test procedure, the tensile tests have been performed by using Zwick Roell 300kN testing machine. Gage length of the specimen is 50mm and the diameter of the gauge is 12.5 mm. All tests have been carried out at room temperature.

Procedure followed in the tests is as follow;

- Measuring gauge diameter of the specimens
- Apply a preload of 100N
- Pulling the specimen till breaking point with constant velocity

Tensile tests have been applied only on the tube materials. Since the raw material diameter of the pin is too small (raw material diameter is 4.5 mm), the new apparatus has been designed but no results were obtained.

The result of the tensile test for the body is shown in the chart below. (Figure 3.4) As shown in the figure, the failure of the tube material obtained at very low strain value which means that the ductility of the tube material is very low.

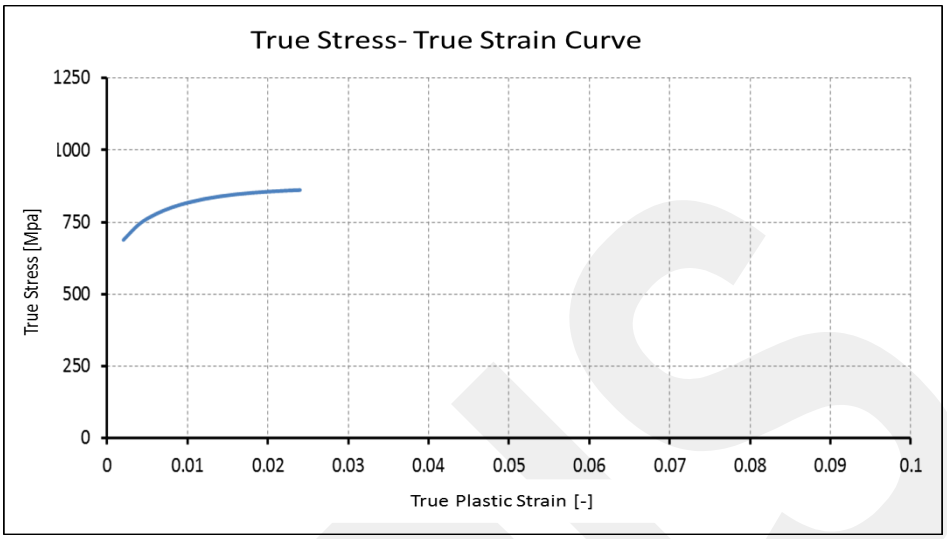

Figure 3.4 True Strain- True Strain Curve obtained from tensile test

In interference fit joint process, the strain values may reach at very high values. A typical metal forming process, this value may reach a value of up to 3. Therefore, the results which obtained from tensile test is not sufficient for the numerical modelling study. However, it can be used for verifying the compression test results.

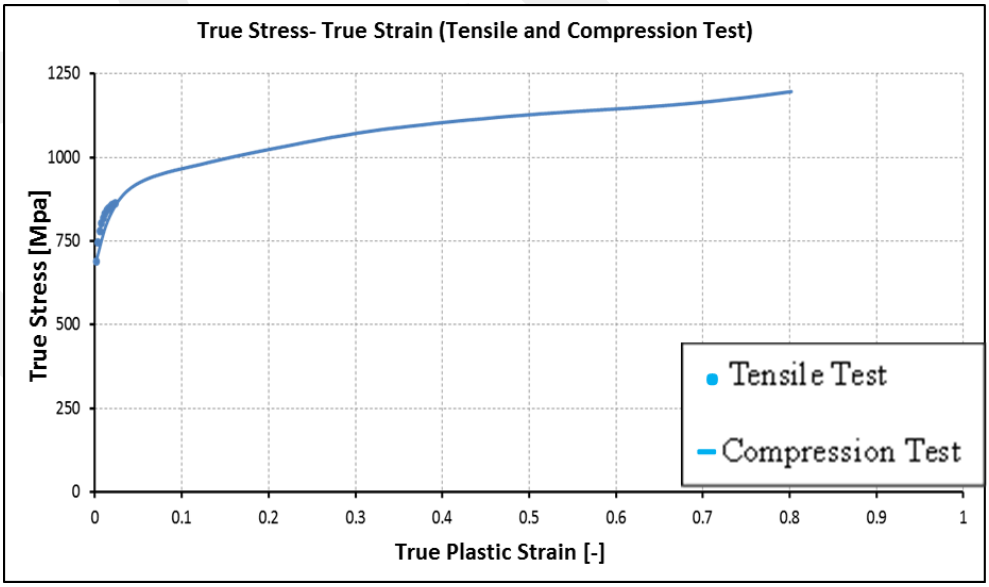

Figure 3.5 Comparison of Tensile and Compression Test on Results (Tube)

As it can be seen in the chart below, (Table 3.2) because of the difference between tensile and compression test is less than 5% which is negligible.

As like compression test, flow curves, obtained from tensile test, were extrapolated by using Ludwik-Hollomon equation. (Eq 3.4). Calculated constants are shown in Table 3.2 for tube material. As mentioned before, only tube's tensile tests could be performed.

Table 3.2 Calculated constants by using Ludwik-Hollomon equation

Tube	(Tensile Test)	(Compression Test)
C (MPa):	1202	923.7
n (-):	0.093	0.029

Analytical models of compression and tensile test flow curves are shown in Figure 3.6. Maximum difference between analytical compression test curve and tensile test curve is less than 4%. Therefore, as illustrated in this figure, the difference can be neglected.

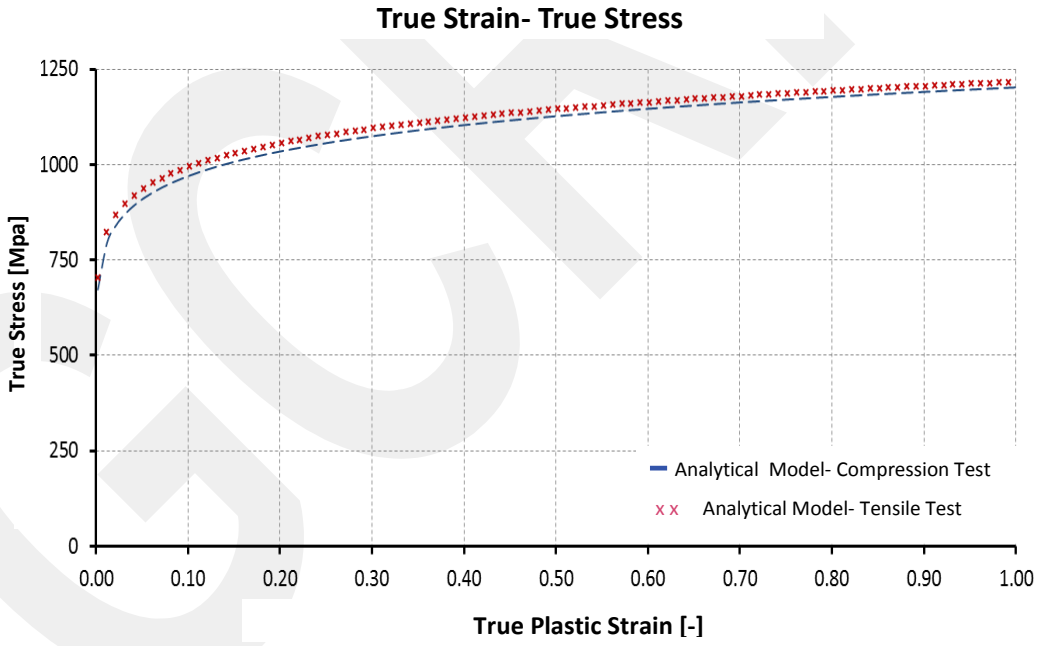

Figure 3.6 Comparison of Tensile and Compression Test (Tube)

Tube and pin material which are used in interference fit joint studies have been investigated. Tensile test and compression test have been performed.

According to compression test results, as mentioned in compression test subsection, work hardening behaviors of the materials are significantly different. In

tensile test results, it can be seen that the ductility of the tube material is too low. In conclusion, during the process; while tube deforms elastically, pin undergoes plastic deformation mainly.

After performing material characterization tests, it can be useful to determine the boundary conditions of the interference fit process. These characterization results help to understand material behavior, other parameters and conditions are specified in next section.

3.2 Determination of the Boundary Conditions

Interference in an interference fitted assembly provides tight intimate contact between mating parts, held permanently by the frictional force produced by the contact pressure between the mating parts. Broadly, there are three types of fits based on amount pin-tube interference; clearance, transition and interference fits. The clearance fit allows some relative motion, while the interference fit provides a tight joint between the two mating parts. This study focuses on interference fit.

To determine and understand the process mechanics, some parameters are specified and examined individually. In interference fit process, these parameters which are shown below can affect the system.

Table 3.3 Parameters that affect the process

Material Properties	Interference Fit Value	Friction	Geometric Properties of Materials
•Elastic Modulus •Stress-Strain Curve	•Maximum •Average •Minimum	•Friction Coefficient •Process Velocity	•Tube (Radius, Angle etc) •Pin (Radius, Angle etc.)

To specify the effects of the parameters on the system, joining trials have been performed. Experiment program was prepared by taking into account actual injection system process.

3.2.1 Joining Trials

Three separate geometries are examined to make the process more understandable. The chosen geometries varied simple to complex form. The geometries are, axisymmetric pin-tube geometry which is example for simple geometry, relatively

complex filter-tube geometry (the only change is pin geometry) and actual process geometry which are shown in Figure 3.7 in schematically form. To avoid the confusion of these geometrical variables, they are named by more understandable ones and showed in mini-chart below.

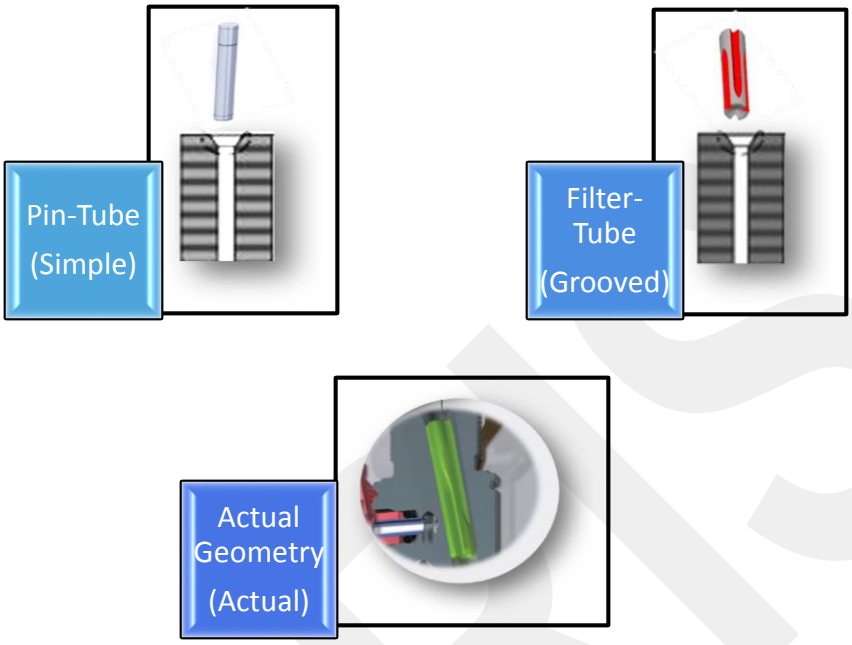

Figure 3.7 Geometry which are used in this study

3.2.1.1 Pin-Tube Geometry (Simple Geometry)

The interference fit process has been simplified inspired by the actual process. The first considered geometry is the simplest which has tried to be solved as two-dimensional problem. Tube and pin geometry is designed as axisymmetric (two dimensional problem). Dimensions of the pin and tube are shown in Figure 3.8. The critical dimensions for tube and pin, which cause interference, are highlighted in this figure.

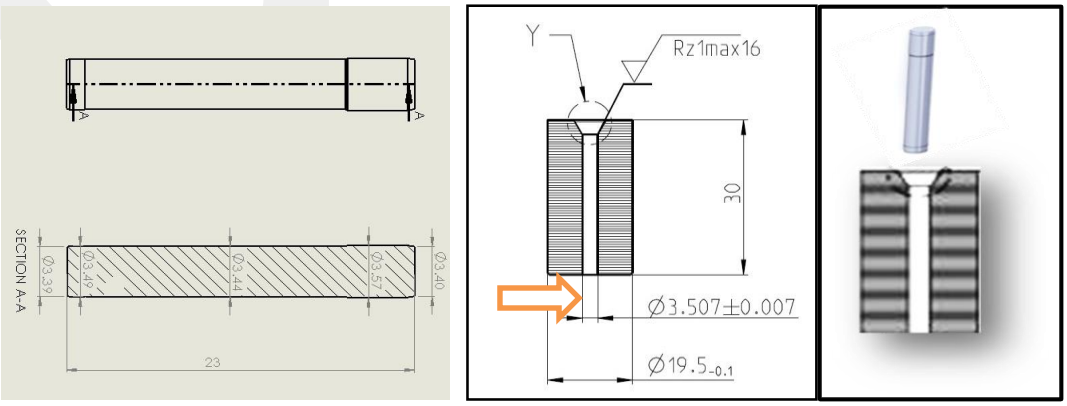

Figure 3.8 Dimensions of the pin and tube (Simple Geometry)

In this section details of both geometries along with physical trials are described below. Analytical and numerical experiments will be mentioned in next chapter. Interference values are obtained by using manufacturing tolerances. All of the dimensions are between these tolerances which are shown in following figure.

3.2.1.2 Filter-Tube Geometry (Grooved Geometry)

Second chosen geometry is filter-tube geometry. The only different part from first one is geometry of pin. Although, this first geometry is useful for studying the basic mechanics of the process, such simple geometry has limited applicability in industrial applications. One example of a geometry used in the industry is the grooved pin, shown in Figure 3.9. To study the mechanics of such joints, in particular joint strength, a three-dimensional model of the grooved filter and the tube was setup. The dimensions of the filter are not shown for confidentiality but schematic view of its shown in Figure 3.9. The filter has three grooves which are filtered out particles in actual system. The critical dimensions for tube and pin, which cause interference, are highlighted in this figure.

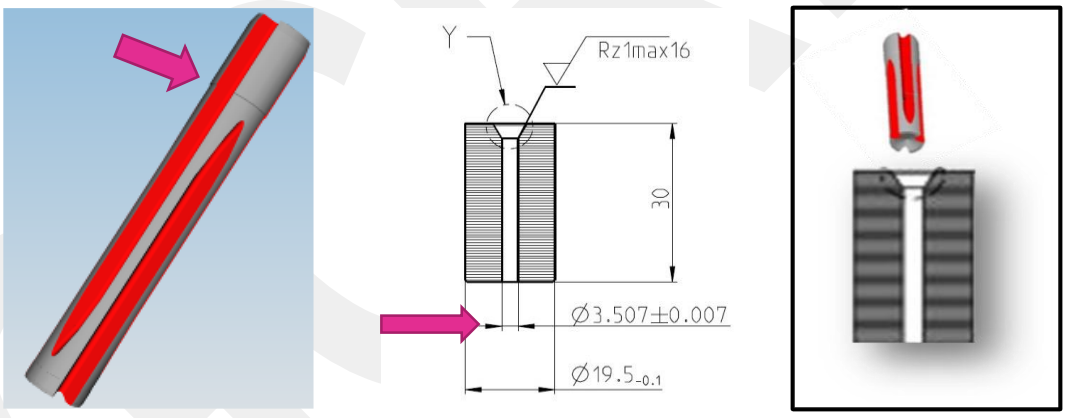

Figure 3.9 Dimensions of the filter and tube (Grooved Geometry)

3.2.1.3 Actual Geometry

The main aim of this study is to examine fuel injection system in mechanical part. Other two geometries and studies are investigated to reach actual process parameters and effects. Actual geometry dimensions are not shown because of the confidentiality. Therefore, it is shown schematically in following Figure 3.10.

After the geometries are determined, the experimental process has been investigated. First, experimental matrix is created. In joining trials part, three different geometries which are pin-tube, filter-tube and actual geometry are examined.

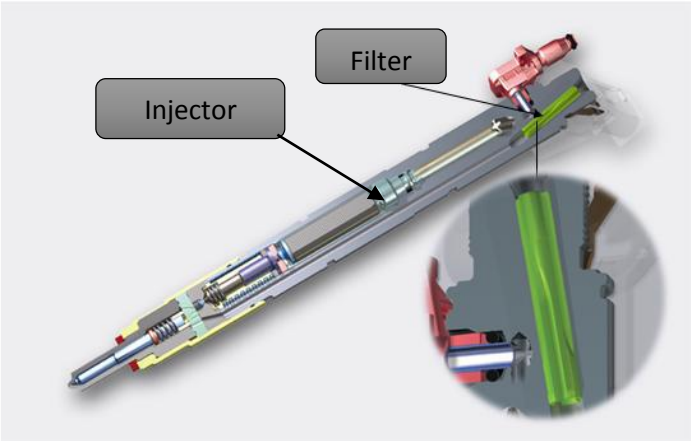

Figure 3.10 Actual process geometry

Details of these geometries are investigated in previous part. To study the joining process, experiments on three pin-tube, three filter-tube and also three actual injector – filter sets were performed, by pushing into the tube at room temperature.

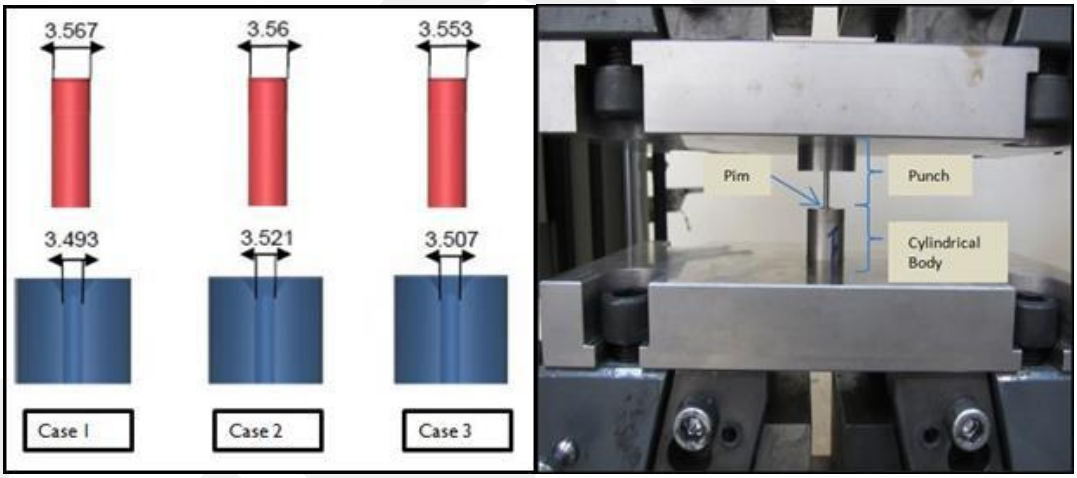

Figure 3.11 Interference fit values of specimens and experimental setup

Three different cases were considered: high, medium and low interference. Specimen geometry and setup is shown in Figure 3.11, and the determined dimensions are given Table 3.4.

Table 0.4 Specimen dimensions and interference fit values of each case

Case	Tube diameter (mm)	Tube height (mm)	Pin diameter (mm)	Pin height (mm)	Interference (µm)
1. High	3.49	30	3.57	23	75
2. Medium	3.51	30	3.56	23	55
3. Low	3.52	30	3.55	23	30

Experiments were performed under controlled conditions on a Zwick Roell uniaxial tension-compression testing machine. To perform these experiments, new apparatus (centering tool) is designed. Because, pin and tube must be centered in order to get accurate results. Designed tool is shown in Figure 3.12.

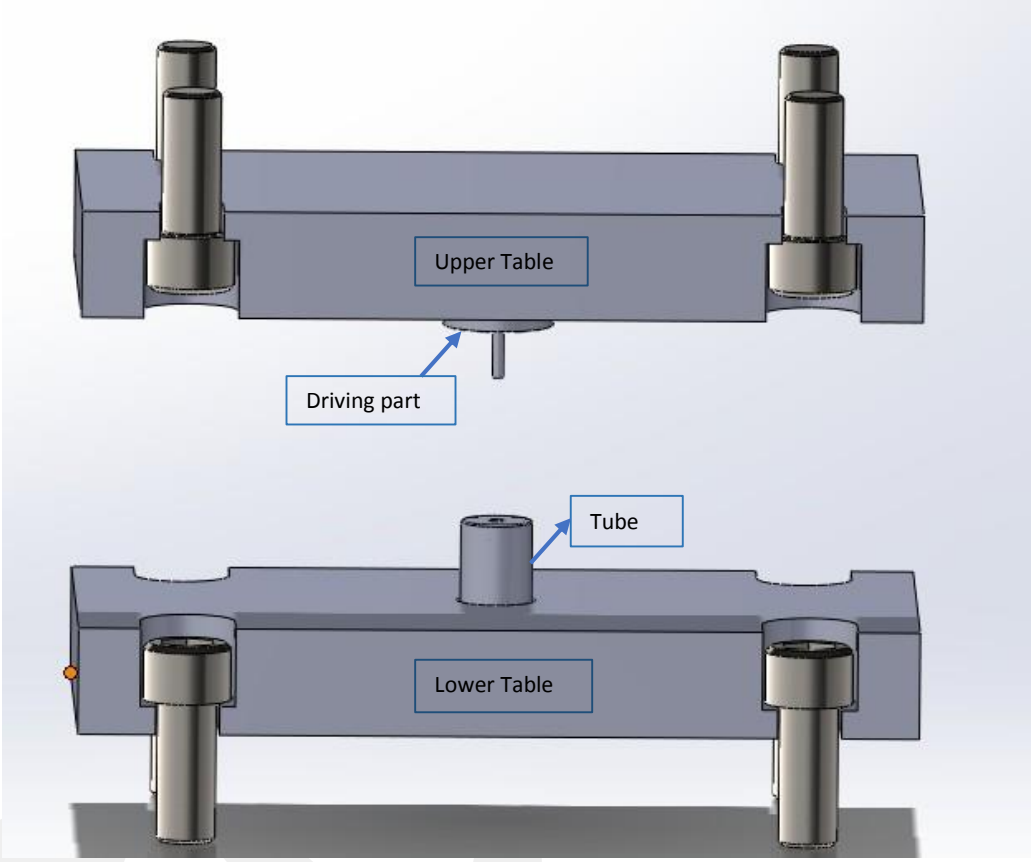

Figure 3.12 Designed tool for performing driving test

After performing these experiments, results are validated and compared with the numerical and analytical results. On the other hand, to increase the performance of the system and investigate the effect of the system parameters, it will be done an extensive study which will be mentioned in 'Analysis' chapter.

In this chapter, it is mentioned about material characterization of the used materials and determination of boundary conditions. In addition, the geometries and design of experiments are summarized briefly. More comprehensive information about the experiments and boundary conditions effect will be given in later sections.

CHAPTER 4

MODELLING

4.1 Introduction

The joining process has been investigated using both experimental and numerical methods. Experiments were described in previous section. This section describes details of the numerical models for each chosen geometry and their validation against experimental results. Before, applying the numerical modelling to solve engineering problems, it's used to simulate some small scale problems and simple cases for which the results are predictable or can be easily obtained for verification. When the simple model is created and gives critical information about the process, it will be easy to understand and come to a conclusion in actual (complex) model.

To model such processes, two basic solution procedures are used; implicit and explicit methods. Implicit method has stable, iterative and high computational effort; on the other hand explicit method is conditionally stable, not iteration and less computational effort. Studies reveal that implicit solver is useful in smaller two dimensional (2D) and axisymmetric problems.

To determine the effects, which are mentioned, ABAQUS, version 6.13.4, finite element analysis solver is used to model the process. ABAQUS has the ability to solve a wide variety of simulation. Abaqus/ Standard uses an implicit finite element solver, such as static, dynamics and thermal.

4.1.1 Simple Geometry

The simple geometry was modelled as two dimensional, axisymmetric problem by using 4-node bilinear full integration axisymmetric elements. Numerical analysis parameters are shown in Table 4.1.

Specimen dimensions have already given previously in Table 3.4. The effects of all parameters have been investigated and these numerical parameters and their effects will be given 'Model Validation' subsection.

Table 4.1 Numerical Parameters of Simple Geometry

Mesh Size	Global element size of 0.1 mm with locally refined mesh of 0.025 mm at pin-tube interface
Mesh Type	Continuum axisymmetric 4-node bilinear full integration element (2D) (CAX4)
Analysis type	Elastic-plastic

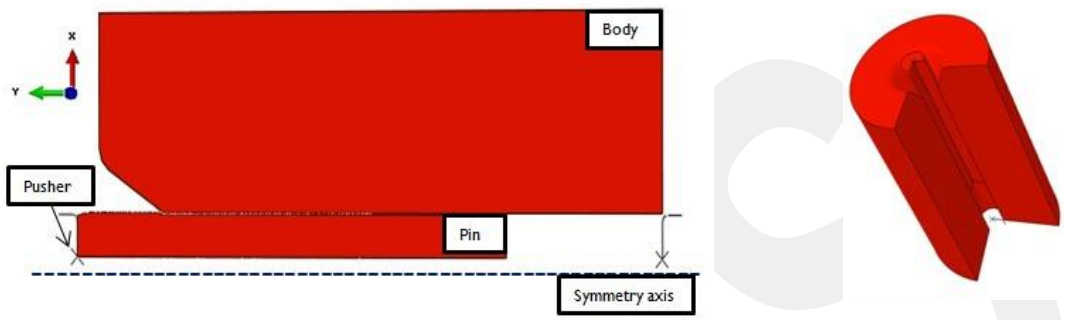

Figure 4.1 Description of Simple Geometry

Figure 4.1 shows that the two dimensional analysis parts. This model is useful in studying the basic mechanics of the process. Friction, contact pressure, disposition of force-displacement curve and effects of numerical parameters can be obtained by using simple model. In other words, this simple model can be used to get prior knowledge about this process. To make the studies more practical and understandable for joining process and, these three geometries are investigated step by step.

4.1.2. Grooved Geometry

The numerical model described in the previous section is used for the simple geometry. However, such simple geometry has limited applicability in industrial applications as mentioned before. Instead of the simple one, the grooved geometry is widely used in the industry as the grooved pin which is shown in Figure 4.2.

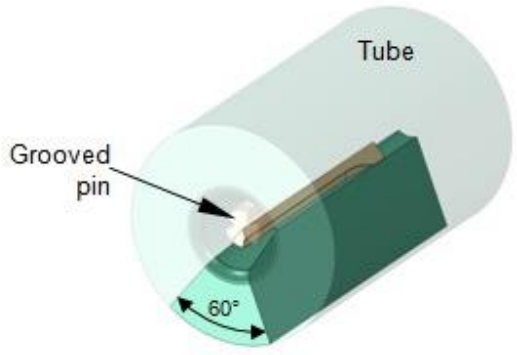

Figure 4.2 Schematic view of grooved geometry

Such grooved pins are used at the fuel inlet in diesel fuel injectors, where the grooves filter out fuel particles. The filter is held in place by a frictional force created through an interference fit with the main body of the injector. In operation, the filter itself is subject to high pressures, which is in high-end fuel injectors can reach the levels of up to 2000 bars. As such, strength of the joint created by an interference fit is critical on the performance of the fuel injector as a whole.

To study the mechanics of such joints, in particular joint strength, a three dimensional model of the grooved filter and the tube was setup. As shown in Figure 4.2, the filter has three grooves, so only one sixth of the geometry is modeled.

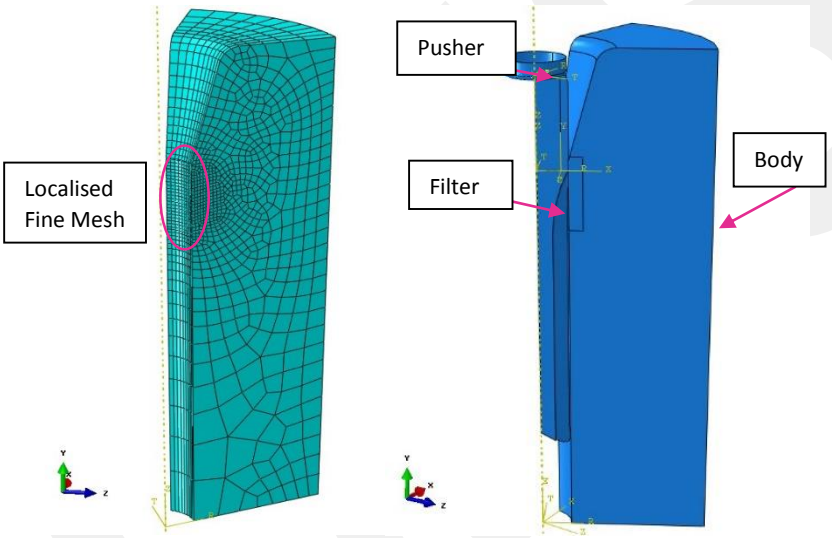

Figure 4.3 Mesh description of the grooved geometry

Figure 4.3 shows the mesh description of the filter and tube. The case of complex geometry was modeled as three dimensional and 8-node-brick element was used to mesh the samples. The following Table 4.2 represents the mesh size and mesh type of the grooved geometry.

Table 4.2Numerical parameters of grooved geometry

Mesh Size	Global element size of 0.1 mm with locally refined mesh of 0.025 mm at pin-tube interface
Mesh Type	Three dimensional (3D) and 8-node brick element (C3D8), Bottom of the filter has been meshed by tetrahedron elements (C3D4)
Analysis type	Elastic-plastic

4.1.3. Actual Geometry

In previous subsection, the numerical model of the grooved geometry was mentioned. The only difference between the grooved and the actual geometry is the tube shape. The other geometrical values are identical for both geometries. For instance, the inside of the tube and injector have same radius, same length and they made from same material. To arrange and compare these two geometry, actual geometry is also investigated by using numerical methods.

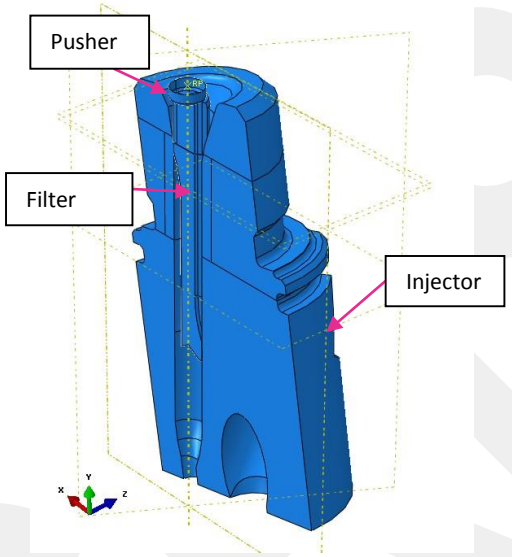

Figure 4.4 Schematic view of actual geometry

As shown in the Figure 4.4 only half of the geometry is modeled. The case of actual geometry modeled as three-dimensional.

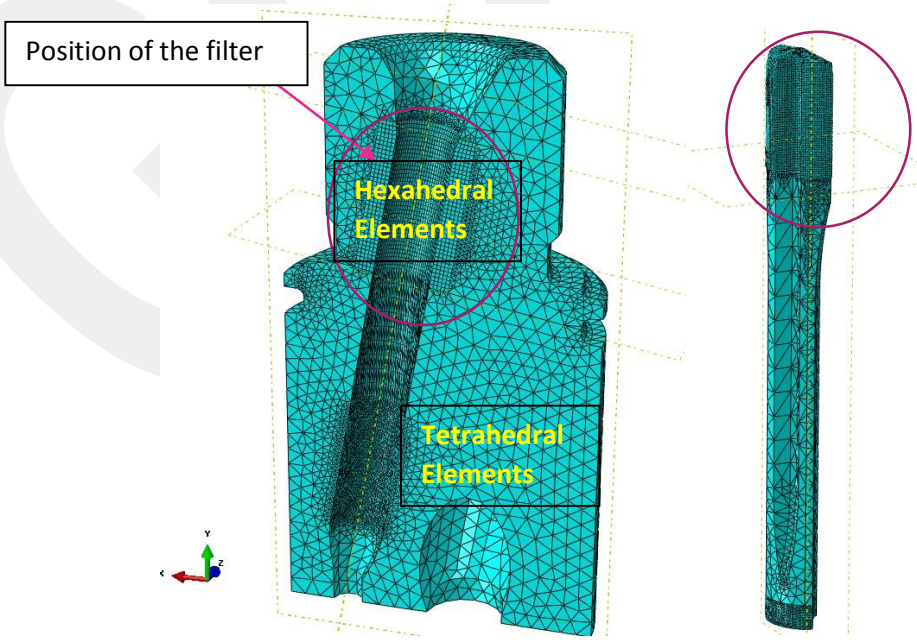

Figure 4.5 Mesh description of the actual geometry

Figure 4.5 shows that the mesh description of the actual process and the position of the filter. Numerical solutions of the simple and grooved geometry have been compared with experimental studies which has been performed by Zwick/Roell Z300 tensile testing device, and also numerical results of actual geometry have been compared with real process results of real production line. Numerical parameters of the actual process have been shown in Table 4.3.

Table 3.3Numerical parameters of actual geometry

Mesh Size	Global element size of 0.1 mm with locally refined mesh of 0.025 mm at pin-tube interface
Mesh Type	Three dimensional (3D) and 8-node brick element (C3D8)is used in critical parts which are top of the filter and filter hole, Bottom of the filter and injector have been meshed by tetrahedron elements (C3D4)
Analysis type	Elastic-plastic

4.2. Model Validation

Finite element model of the joining process is a convenient tool for improving the process. However, before a detailed study of the process is performed, the model needs to be validated.

Model validation was done in two steps. First, a mesh sensitivity analysis was performed, followed by iterations to determine the friction coefficient through comparison with physical trials as described in Chapter 3.

Mesh sensitivity was performed by gradually reducing element size while monitoring the maximum joining force.

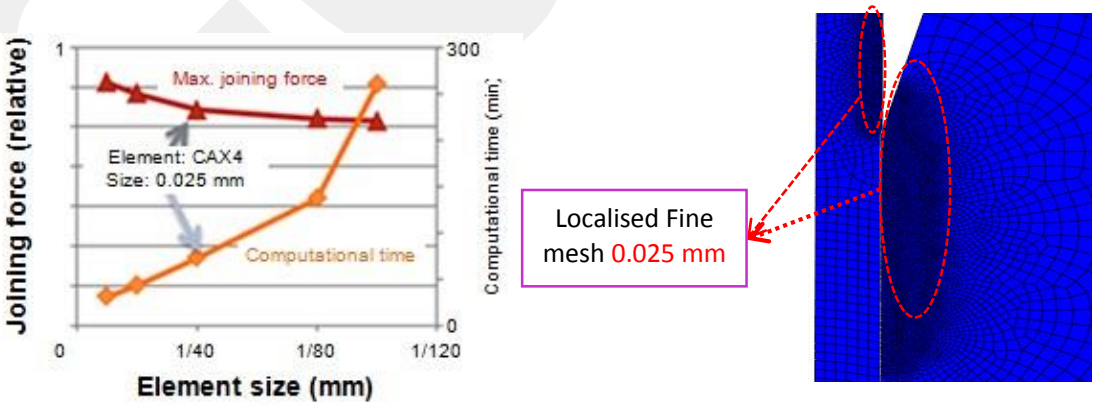

Figure 4.6 Joining force and computational time vs. element size

Figure 4.6 shows the results, a plot of force and computational time against element size. It's seen that as the element size is reduced, the force values converged to a value. However, at the same time, the computational time increases rapidly, as expected.

There is a trade-off between the accuracy of the simulation and the computational time. Element size of 0.025 mm was chosen since any further reduction in element size beyond this point will result in a change of less than 3 %, which is considered as in the acceptable range at this stage.

All of the analyses that described have been performed for a fixed Coulomb friction coefficient of 0.1, a value typically used for lubricated steel to steel contact. However, a set of iterations was done to determine the friction coefficient of the joining process. The friction coefficient of friction was determined as 0.14, for both simple and grooved geometry. Conversely, for actual geometry, the friction coefficient was determined as 0.1. In Analysis Chapter, the friction model and coefficients will be described in a detailed way.

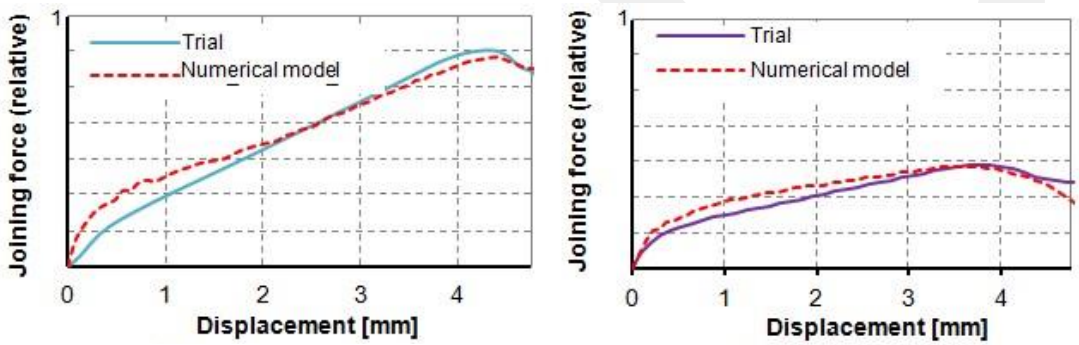

a) Simple Geometry b) Grooved Geometry

Figure 4.7 Force-Displacement Curves for (a) simple geometry, (b) grooved geometry

Taking into account the simple and grooved geometry, the results of numerical and experimental studies are almost identical as shown in Figure 4.7. For the simple geometry; the agreement is to within 10 %; while the grooved geometry the maximum difference is just under 15%. For this stage, it's acceptable but for more accuracy, the model needs to be improved.

CHAPTER 5

ANALYSIS

In analysis chapter, numerous parameters effect will be investigated. As mentioned in Table 3.3, which is located in Chapter 3, parameters that affect the process; material properties, interference fit value, friction and geometrical properties of the materials has been studied by using numerical and experimental methods.

In this section, using the information from both physical and numerical trials, important point of the process is presented. The parameters can be divided into four main titles which are;

- Interference fit value
- Material properties
- Friction
- Geometrical properties

5.1 Interference fit value

In actual process, (diesel injection system) interference fit value varies from 30 μm to 90 μm. In our study, we specified three simple sections for these values which are;

- ✓ Minimum interference: 30 μm - 35 μm
- ✓ Medium interference: 50 μm -60 μm
- ✓ High interference: 70 μm- 90 μm

These parameter studies are repeated for simple and grooved geometry by using numerical and experimental method. Figure 5.1 shows a representative force-displacement curve of joining process. An important observation can be made from this figure.

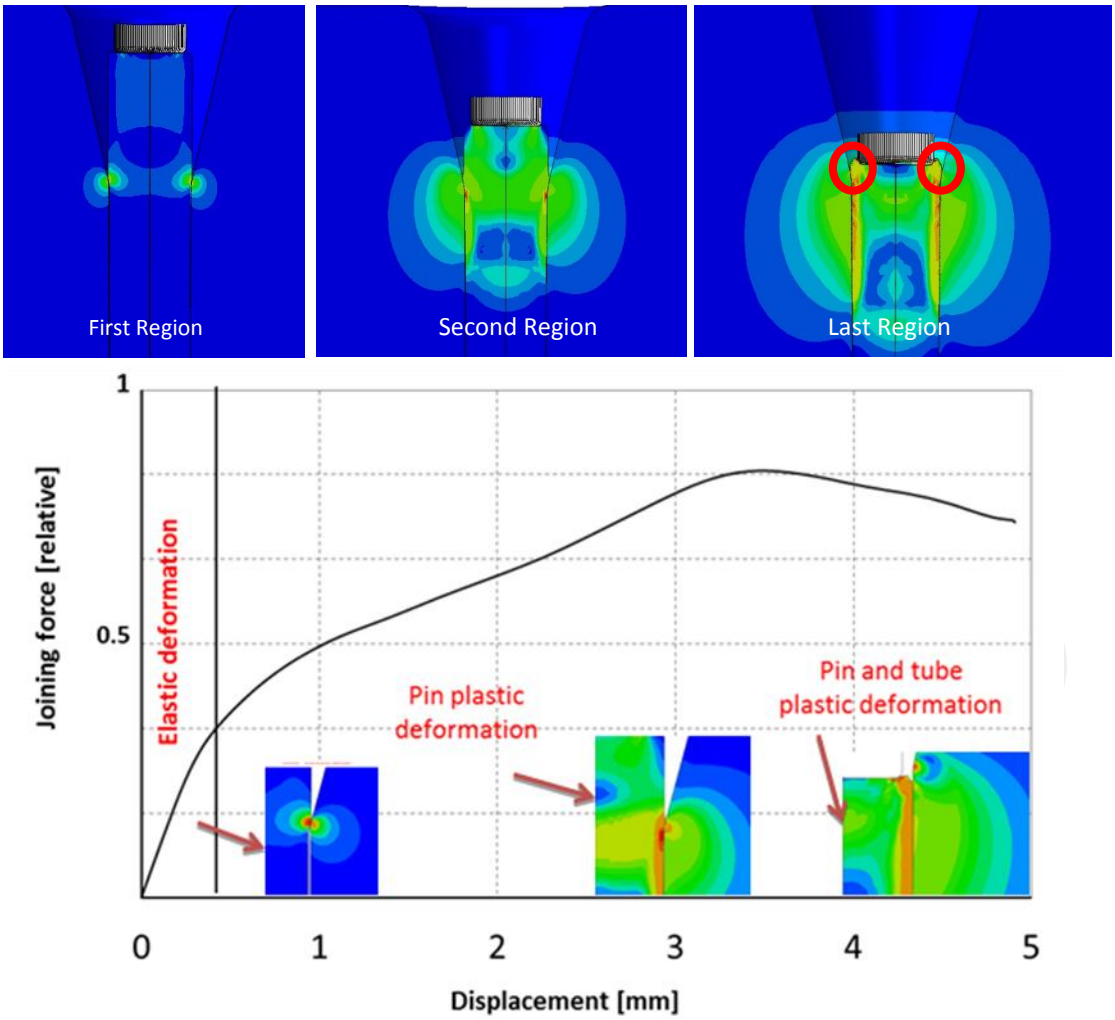

Figure 5.1 Representative Curve of Joining Process

The force curve can be split into three regions;

1. Elastic deformation region: The contact is initialized and the pin touches the tube without permanent deformation.

2. Plastic deformation region: The pin deforms plastically and the contact between the pin and tube gradually increases as the pin is pushed into the tube, leading to an almost linear increase in the joining force.

3. Last region: The region where both pin and tube deform plastically, leading to a drop in the joining force. This region tells, when the pin touches the tube with permanent deformation, the upside of the pin gets larger and the effective interference between tube and pin is decreased. For this reason, the joining force decreased.

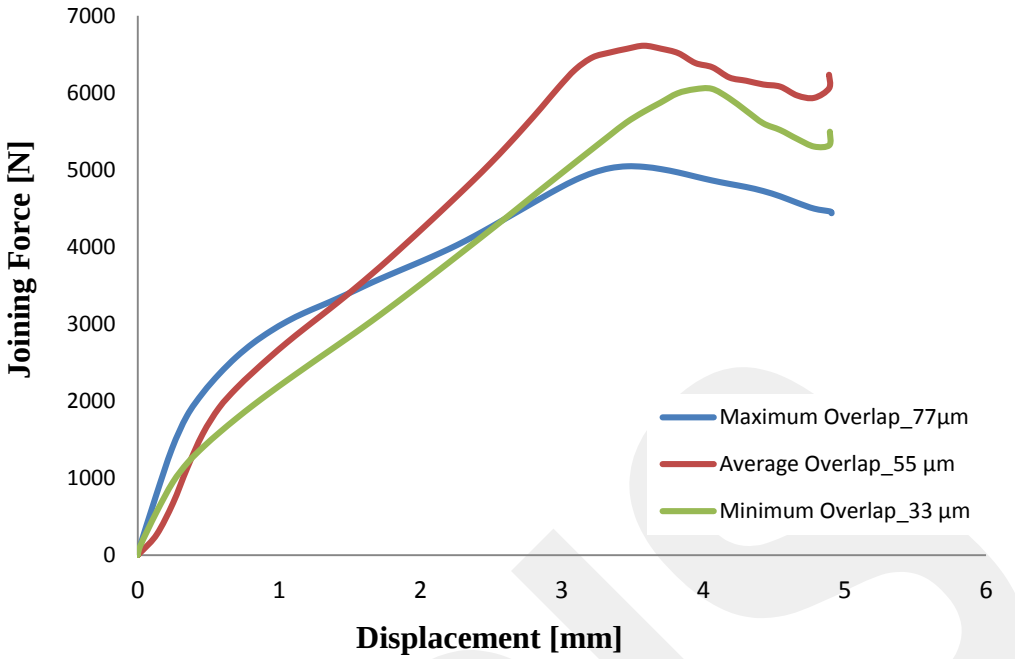

Figure 5.2 Force-Displacement Curves of Simple Geometry with Different Overlap Values (Experimental)

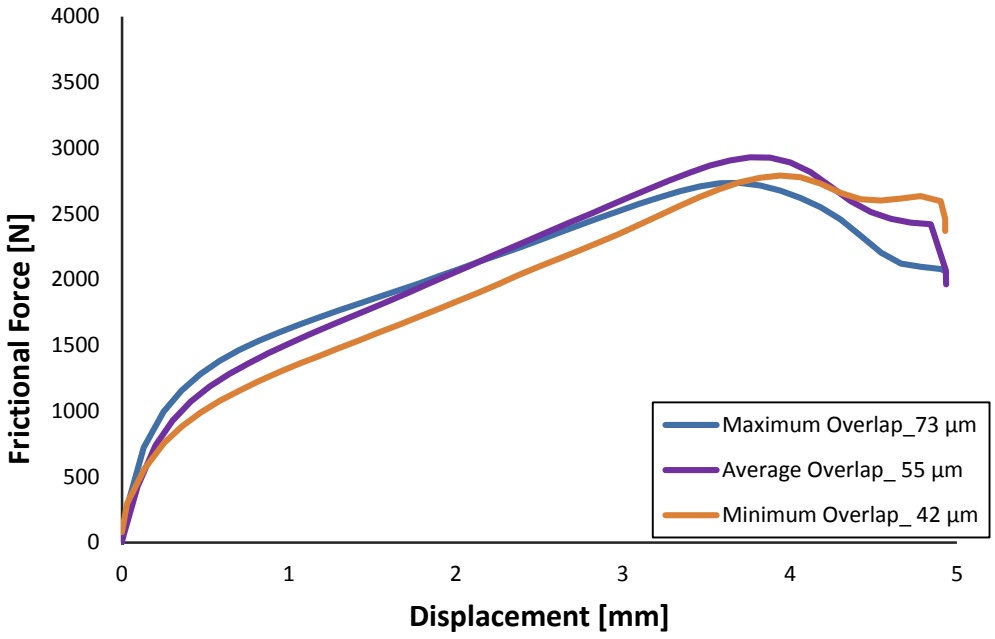

Figure 5.3 Force-Displacement Curves of Grooved Geometry with Different Overlap Values (Experimental)

Figure 5.2 shows the force- displacement curves for simple geometry, for three different interference values; 33 μm -55 μm -77 μm.

Figure 5.3 shows the force- displacement curves for grooved geometry, for three different interference values; 42 μm -55 μm -73 μm. One key conclusion to be drawn from both figures is that maximum interference does not provide maximum joint strength; instead the joint force seems to reach the maximum around the average overlap value. This is expected, since at high interference values, tube tends to deform plastically at an early stage, reducing frictional force holding the two parts together.

Finally, comparing the force for simple geometry and grooved geometry, it's seen that the friction force in the grooved geometry is approximately one half of the force for simple geometry. The ratio of the two forces is in direct proportion to the pin- tube contact area.

5.2 Material Properties

Modulus of Elasticity and Yield strength of the materials has been investigated in this sub-section.

5.2.1 Young's Modulus

Young's Modulus and yield strength are considered as material properties to determine its effect on the maximum load of the joining. At first, by using ABAQUS, finite element analysis program, Young's modulus effect has been investigated. In this study, to determine the elasticity modulus of pin and tube the test has been performed and the value was found 207 GPa for both.

Modulus of elasticity values of body and filter materials are changed from 160 GPa to 250 GPa to investigate its influence on the process.

Figure 5.4 shows that when the elasticity modulus of pin and tube is decreased, the process reaches to maximum force. The only difference of these four curves is the elastic modulus value. In a same way, minimum force is obtained for higher elastic modulus values.

This study has been done to investigate the effect of Modulus of Elasticity. According to the results, if the material will be decided to change in the future, elastic modulus effect also can be taken into account.

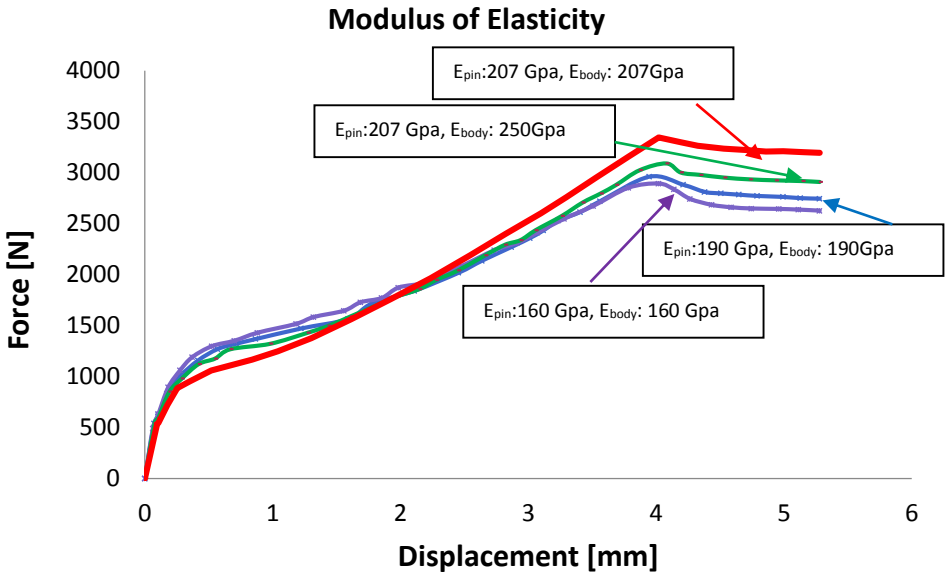

Figure 5.4 Force- Displacement Curves for different Elastic Modulus values

5.2.2 Flow Curve

The body material which is used in injector part, has been supplied by two different suppliers. The flow curves which belong to two different suppliers are shown in Figure 5.5.

As shown in this figure, the difference between two suppliers is 15%. To avoid the failure of the process which may occur because of this difference, finite element analysis also has been performed to ensure how it affects the joining force.

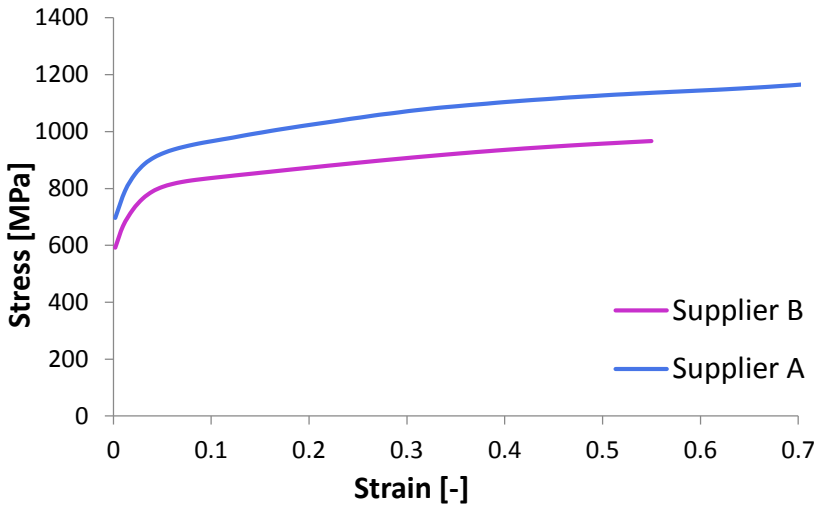

Figure 5.5 Flow curves of body material which are supplied by different suppliers

However, this difference is in the acceptable range specified by the firm. To prevent the effect of different material flow curves, only one supplier's material has been used for all the experimental works.

5.3 Geometrical Properties

In order to understand the effects of the geometrical properties on the process, following studies have been done.

5.3.1 Body Entrance Angle

In order to compare and to see the difference between geometrical changes, the body entrance angle has been changed. Two models are created and analyzed by using ABAQUS FEA program; also experiments have been performed to compare numerical results.

Entrance angle have been decided by taking into account two different injection system angles. Body entrance angle is shown in Figure 6.6. Experimental matrix has been designed which represents in Table 5.1.

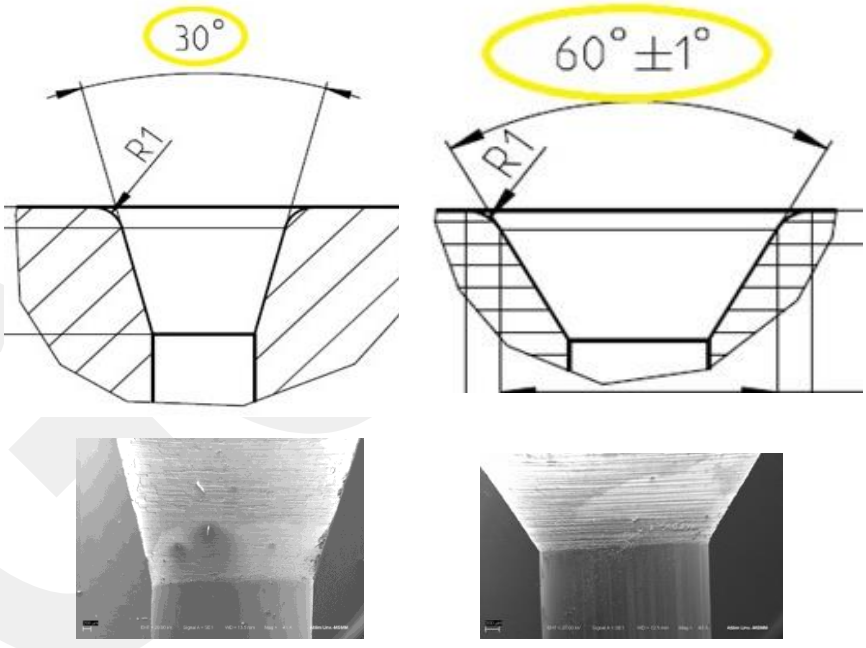

Figure 5.6 Schematic view of body entrance and values

Experiments were performed under controlled conditions on a Zwick Roell Uniaxial Tension-Compression Testing Machine. Each experiment were repeated two times and each pin-tube set was carefully centered by using a centering tool.

Table 5.1 Body Entrance Angle vs Overlap Values

Entrance Angle	Minimum Overlap	Average Overlap	Maximum Overlap
30º	39 Mm	64 µm	86 µm
60º	37 Mm	63 µm	86 µm

✓ Maximum Overlap - 30º /60º entrance angle

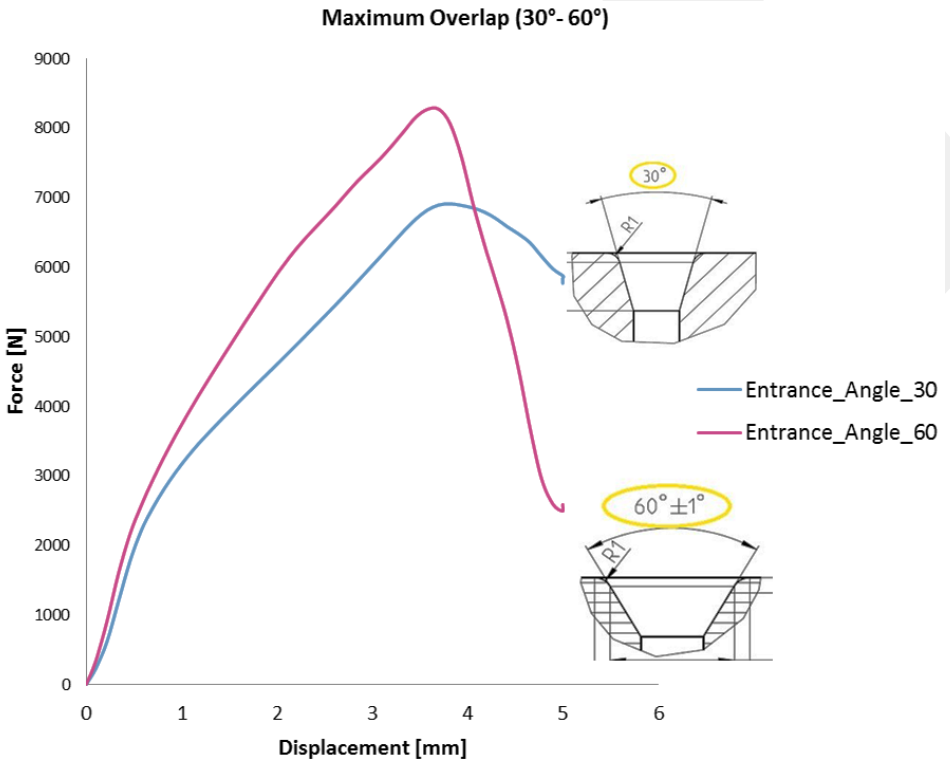

Figure 5.7 Force Displacement Curve for Different Entrance Angle (Maximum Overlap, Experimental Results)

As shown Figure 5.7, there is a difference between 30 º and 60 º entrance angle curves. Maximum joint force and last joint force are slightly different to each other. The experimental results of 30 º geometry, the maximum joining force reached lower value than the 60 º geometry. The 60 º geometry, the body entrance radius value increased so it becomes a sharp edge. When the pin started to enter body, at an early stage the joining force increased. However, at the middle stage of the joining, the pin deforms and the diameter of pin decreased. In other words, the interference value decreased. As shown in the Figure 5.7, last part of the joining process, the force value

decreased. The reason of the reduction in force was the decrease of the interference value.

- ✓ Average Overlap - 30º /60º entrance angle (66 µm)

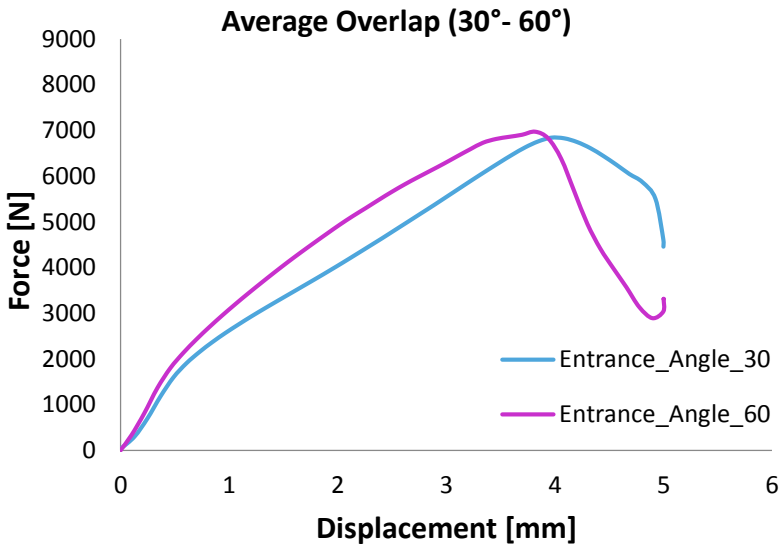

Figure 5.8 Force- Displacement Curve for Different Entrance Angle (Average Overlap)

- ✓ Minimum Overlap - 30º /60º entrance angle (39 µm)

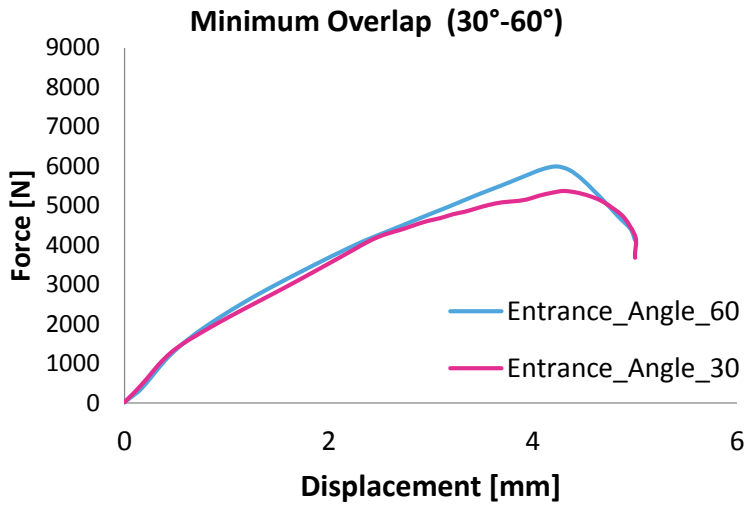

Figure 5.9 Force- Displacement Curve for Different Entrance Angle (Minimum Overlap)

As can be seen in Figure 5.8, while the last joint force reaches a value up to 3000 N in 60º entrance angle. Body which has 30 º entrance angle, this value reaches 4600 N.

As shown in the Figure 5.9, while the last joint force reach a value up to 3000N in 60 º, body which has 30 º entrance angle reaches a value 4000N.

To sum up, as expected when the interference value is increased, maximum joint force also increases. Also the important conclusion is, while the entrance angle increased, the last joint force is decreased. The following table shows the maximum joint force and last joint force values.

Table 5.2 Maximum and Last Joint Force of Different Entrance Angle

30 ° Overlap Value	60 ° Overlap Value	30° Maximum Force	60° Maximum Force	30° Last Joint Force	60 ° Last Joint Force
86 µm	86 µm	~7000 N	~8100 N	~6000 N	~2700 N
64 µm	64 µm	~6845 N	~7000 N	~4500 N	~3000 N
39 µm	37 µm	~5100 N	~5000 N	~4000 N	~4000 N

Holding force also changes by varying entrance angle. While the entrance angle is increased, holding force is decreased dramatically. As can be seen in Figure 5.7, Figure 5.8 and Figure 5.9, increasing the body entrance angle affects the holding force and slopes of the force- displacement curves.

5.3.2 Body Entrance Radius

During the examination of the process, simulations and experiments show that, the first contact point is body entrance radius.

To see this effect, simulation has been done by changing entrance radius. In the real process, this value is 0.2. This value has been changed to two different values which are 0.7 and 0.8.

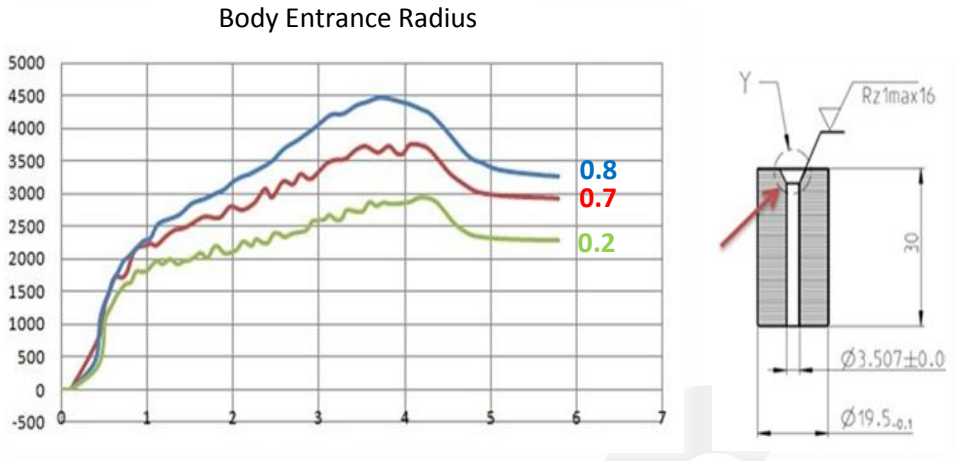

Figure 5.10 Force-Displacement Curve for Different Body Entrance Radius

The body entrance radius affects force directly. Figure 5.10 shows while the radius is increased, joining force is also increased.

5.4 Friction

Friction is one of the most important parameters in joining processes. It affects material flow in the die, forming load, strain and stress distribution.

The range of the coefficient of friction in different joining applications is not well known and factors affecting variation are ambiguous. In this section, a variable coefficient of friction depending on the contact interface conditions is applied. Instead of using comparatively simple friction model, Coulomb, friction models proposed by Wanheim-Bay were used to simulate joining force. The FEA results are compared with the experimental results.

Friction, in a simple manner, can be described as 'surface resistance to the relative sliding or rolling motion'. On the contrary to its simple definition, friction is a very complex phenomenon and includes several parameters that interact with one another such as; sliding speed (joint), contact pressure between body and pin, surface roughness, material properties, temperature and lubrication condition.

In joining process; friction has critical importance since it affects the forming force, material flow, and as result of these product. In addition to process, friction model is one of the key boundary conditions in finite element simulations. Among the various friction models in literature which one is of higher accuracy is still unknown and controversial [17].

In this study, two different friction models are Coulomb Friction Model and Wanheim-Bay (General) Friction Model have been investigated.

5.4.1 Coulomb Friction Model

When surfaces are in contact, they usually transmit shear as well as normal forces across their interface. Thus, the analysis may need to take frictional forces, which resist the relative sliding of the surfaces, into account. Coulomb Friction is a common friction model used to describe the interaction of contact surfaces.

The model characterizes the frictional behavior between the surfaces using a coefficient of friction μ. [21]

$$\tau = \mu p \qquad Eq.5.1$$

Where μ is the coefficient of friction, p is the contact pressure between the two surfaces. This equation gives the limiting frictional shear stress for the contact surfaces. The contacting surfaces will not slip (slide relative to each other) until the shear stress across their interface equals the limiting frictional shear stress, μp. For most surfaces μ is normally less than unity. Coulomb friction can be defined with μ or τ. [21]

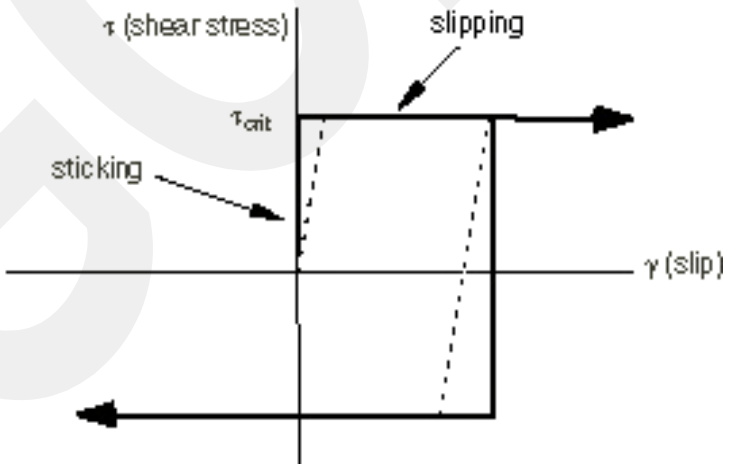

Figure 5.11 Frictional Behavior [21]

Figure 5.11 represents the behavior of the Coulomb friction model: it exists zero relative motion (slip) of the surfaces when they are sticking. [21]

In joining process, the Coulomb friction model is implemented the Finite Element Analysis program and the results have been investigated and compared to experimental data.

All of the analyses described have been performed for a constant Coulomb friction coefficient of 0.1, a value typically used for lubricated steel to steel contact. In this step, however, a set of iterations was done to determine the friction coefficient. The friction coefficient was determined through comparison with the results of joining trials for both simple and grooved geometry.

At the beginning of the friction model studies, different Coulomb friction coefficients are used to understand which coefficient range is compatible with the joining experiments. Friction coefficients are varied from 0.1 to 0.18.

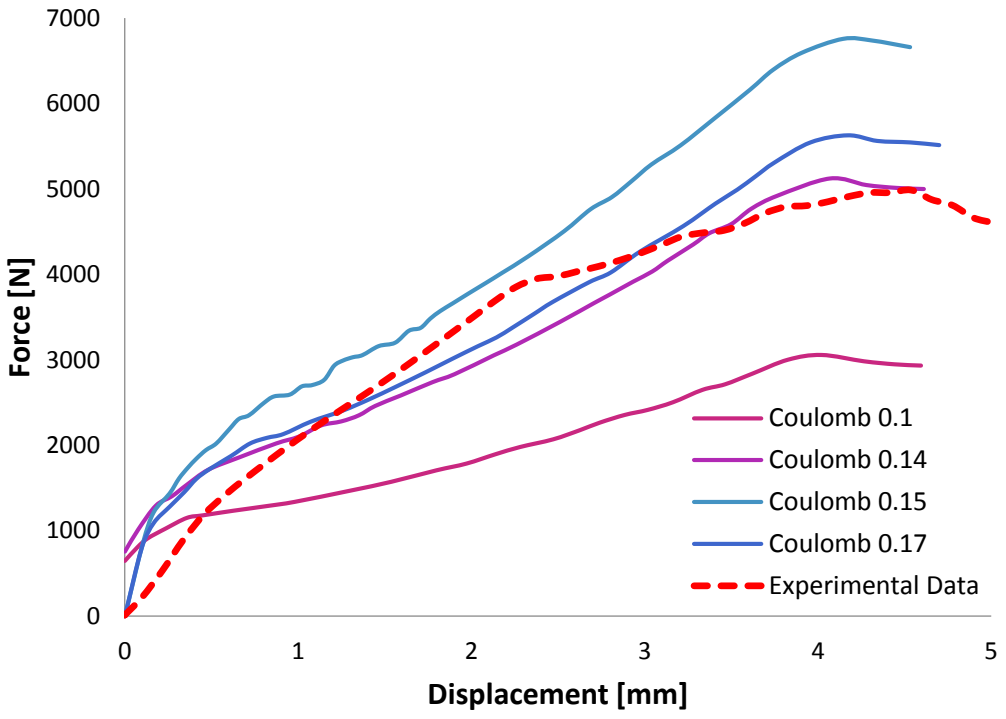

Figure 5.12 Comparison of different friction coefficient with experimental result

When the different coefficients are applied to the numerical model, it's seen that the experimental results, which is highlighted with red dashed lines, remains between values of 0.1 to 0.15. For obtaining more accurate solutions, the friction model and determining of friction coefficient studies are done for more different interference fit

values, and other conditions such as different body entrance angle, different geometries (simple, grooved and actual process).

The different friction coefficients are applied to numerical model for simple geometry which has 33µm interference fit value. At first, experiments were repeated three times for the same interference value to obtain more accurate force range. After performing physical trials, numerical model was created by using same overlap value and geometrical properties, because the variety of the parameters affects the solutions critically.

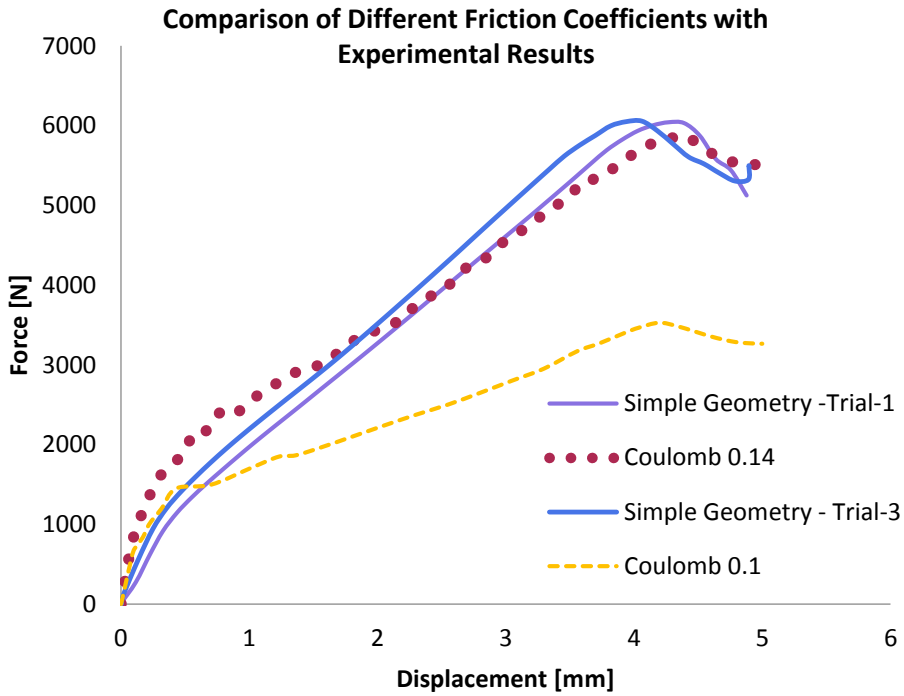

Figure 5.13 Comparison of different friction coefficient with experimental result for simple geometry (Minimum Overlap)

The physical trials results and numerical solutions are given at Figure 5.13. At the figure, the physical trials curves are followed almost the same trend. The difference between maximum joining forces of these two trials is approximately 2%. Physical trials are compatible to Coulomb friction coefficient of 0.14.

In further studies, experimental trials of the grooved geometry and numerical solutions are compared to each other and the friction coefficient value, 0.14, also used for this system. Experiments are repeated two times and numerical model is also created by using grooved filter geometry and interference fit values of body and filter.

The physical trials and numerical model is also applied for grooved geometry which has 55µm interference fit value. In this Figure 5.14, there is a difference (%10) between repeated experiments.

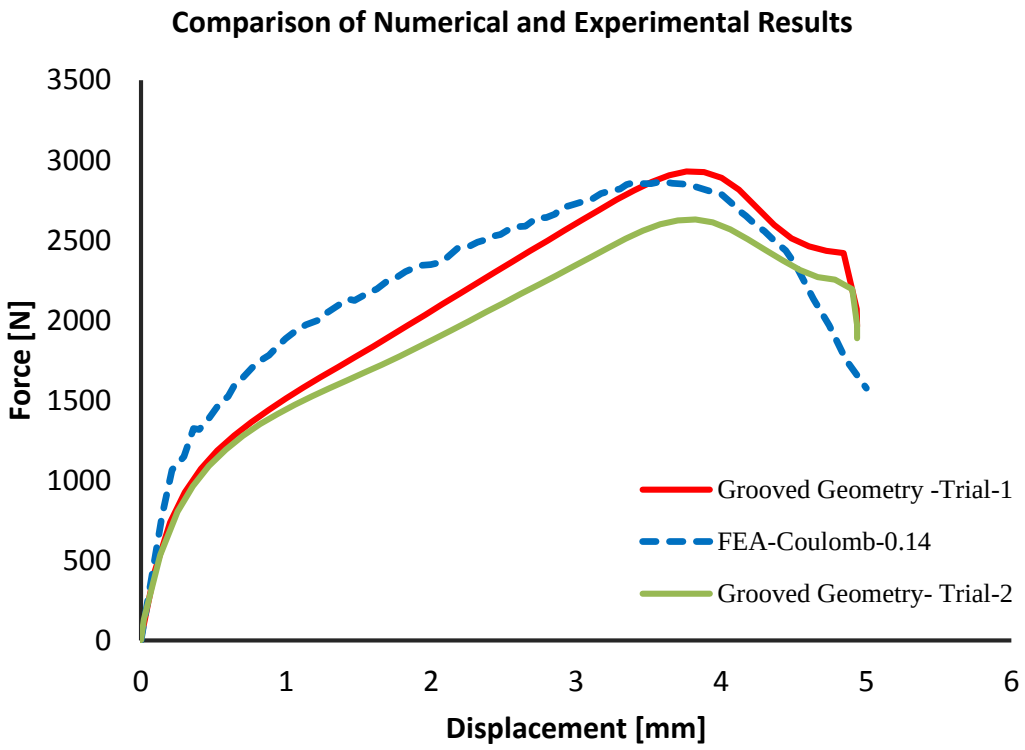

Figure 5.14 Comparison of different friction coefficient with experimental result for grooved geometry

This difference may have occurred due to the diameter measurement of the grooved filter geometry. As mentioned before, filter has three grooves and the dimensions of the filter could not be measured properly. It is seen that the curve of numerical solution of the grooved geometry has been passing between these experimental curves. The friction coefficient value, 0.14, is convenient for this geometry. The first part of the numerical and experimental curves has a difference. The reason of this difference may be explained by using Figure 5.14. As also shown in this figure, these area is elastic region of the process. Modulus of elasticity could cause this difference.

Friction coefficient studies are also applied the trials which has 30° body entrance angle for simple geometry. These trials interference fit values ranges from 84 µm to 88µm.

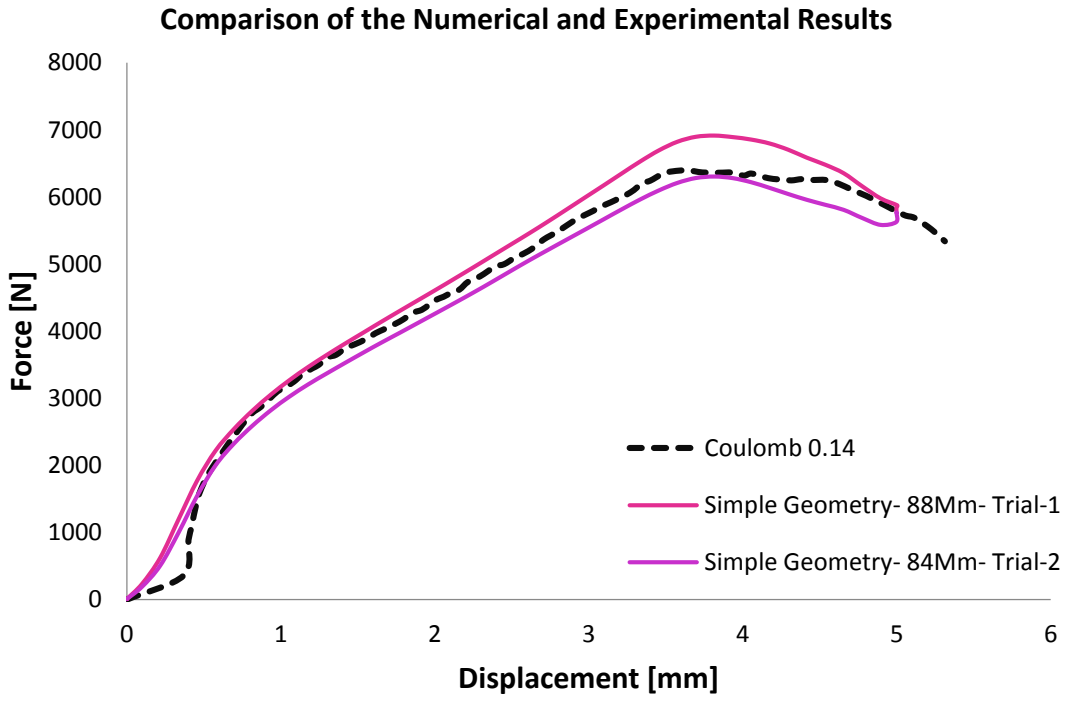

Figure 5.15 Comparison of different friction coefficient with experimental result for 30° body entrance angle (simple geometry, maximum overlap)

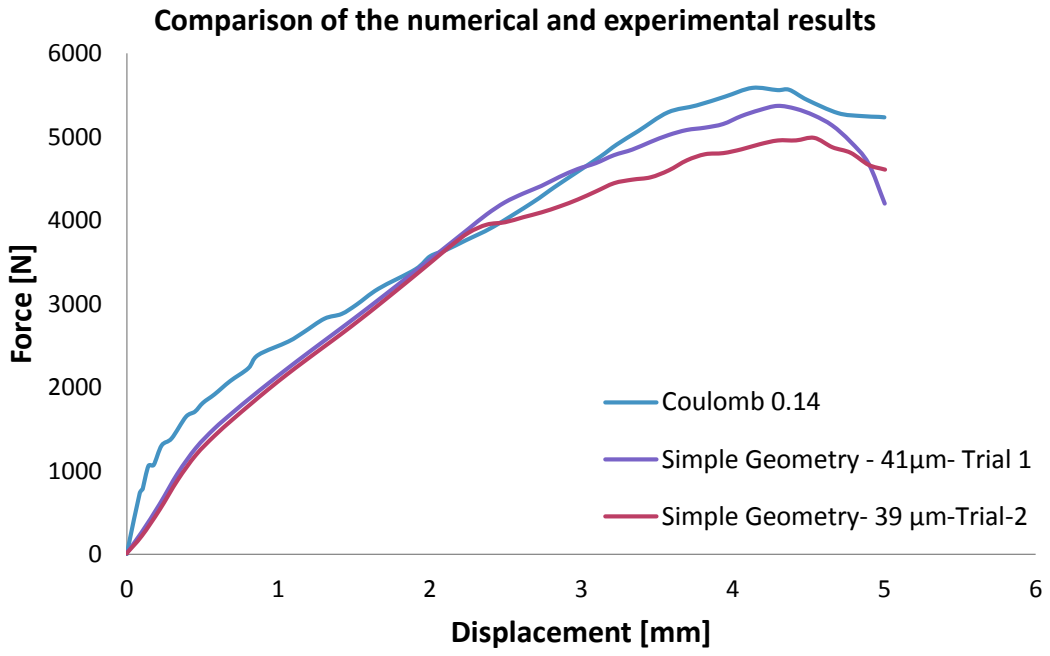

Figure 5.16 Comparison of different friction coefficient with experimental result for 30° body entrance angle (simple geometry, minimum overlap)

Maximum interference fit trials which is varied from 75µm to 90µm has been done and friction coefficient study is shown in Figure 5.15. Because of having limited number of sample for these group, these experiments samples were selected within a range between 80µm- 90µm. As expected, the friction coefficient, 0.14, is fitted well with the experiments.

This study has been also repeated for minimum overlap of the 30° body entrance angle samples. The values were varied from 39 µm -41 µm.

As shown in this figure (Figure 5.16), the friction coefficient, 0.14, agrees well with the physical trials.

In conclusion, the Coulomb Friction Model is applied to numerical model of simple and grooved geometry. In experimental parts, the dimensions are measured critically but the measurement of the grooved filter is hard. Also it is necessary to measure the full-length of the pin and grooved filter. The simulation and experiments show that small changes of the dimensions of the joining parts result in a large variation. Results show that the friction coefficient and the friction model agree well with the experimental results. In following subsection, another friction model which will be mentioned in detailed has been applied to numerical model and compare with to actual process results.

Actual process will also be compared with experimental results of the grooved geometry to see if the difference exists to each other. Results will be discussed in following section.

5.4.2 Wanheim- Bay (General) Friction Model

A study of Wanheim [19], Amonton's friction law can not be implemented when the normal pressure is higher than yield stress of the material. It was also mentioned about the importance about following issues; the frictional stress as a function of normal pressure, surface properties, lubrication and length of joining. To consider these issues, Petersen, Wanheim and Bay developed a friction model which is named General Friction Model. The model can be thought as an updated model of constant friction [18].

$$\tau = f\alpha k \qquad Eq.5.2$$

Where;

- ✓ τ : Friction Stress
- ✓ f: Friction Factor (0≤f ≤1)
- ✓ α : Ratio of real contact to the apparent contact area
- ✓ k : Shear Flow Stress (Yield Stress in pure shear)

The real contact ratio α and frictional stress τ are determined as functions of the nominal pressure q/σ_0 and friction factor f, given in Figure 5.17.

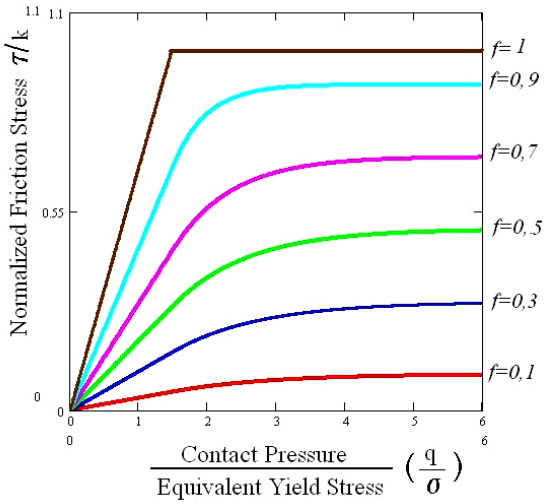

Figure 5.17 Normalized friction stress as a function of nominal pressure and friction factor for Wanheim Bay Friction Model

The model assumes that the friction to be proportional to the normal stress at low normal pressure (q/σ_0<1.5), but going towards a constant value at high normal pressure (q/σ_0> 3). These two ranges are being combined by the intermediate transition region as shown in Figure 5.17.

$$\frac{\tau}{k} = \frac{\tau^*.p/\sigma_0}{k.p^*/\sigma_0} \quad for \quad p/\sigma_0 \leq p^*/\sigma_0 \qquad Eq.5.3$$

$$\frac{\tau}{k} = \frac{\tau^*}{k} + \left(f - \frac{\tau^*}{k}\right).\left[1 - exp\frac{\left(\frac{p^*}{\sigma_0} - \frac{p}{\sigma_0}\right) * \frac{\tau^*}{k}}{\left(f - \frac{\tau^*}{k}\right) * \frac{p^*}{\sigma_0}}\right] for \frac{p}{\sigma_0} \geq p^*/\sigma_0 \qquad Eq.5.4$$

Where σ_0 is the flow stress, τ/k and p/σ_0 are called the dimensionless friction stress and the dimensionless normal pressure respectively. The limit of proportionality between friction stress and normal pressure ($\tau^*$and p*) is defined by:

$$\frac{\tau^*}{k} = 1 - \sqrt{1-f} \qquad Eq.5.5$$

and,

$$\frac{p^*}{\sigma_0} = \frac{1 + \frac{\pi}{2} + arccosf + \sqrt{1-f^2}}{\sqrt{3}(1 + \sqrt{1-f})} \qquad Eq.5.6$$

The calculations are done by using joining process input. Numerical simulations show that maximum contact pressure reaches 3000 MPa. So this pressure value is taking into account whole the calculation. Figure 6.15 shows the calculated friction coefficient – contact pressure curve. Each curve has calculated by using different friction factor value (range between 0 to 1).

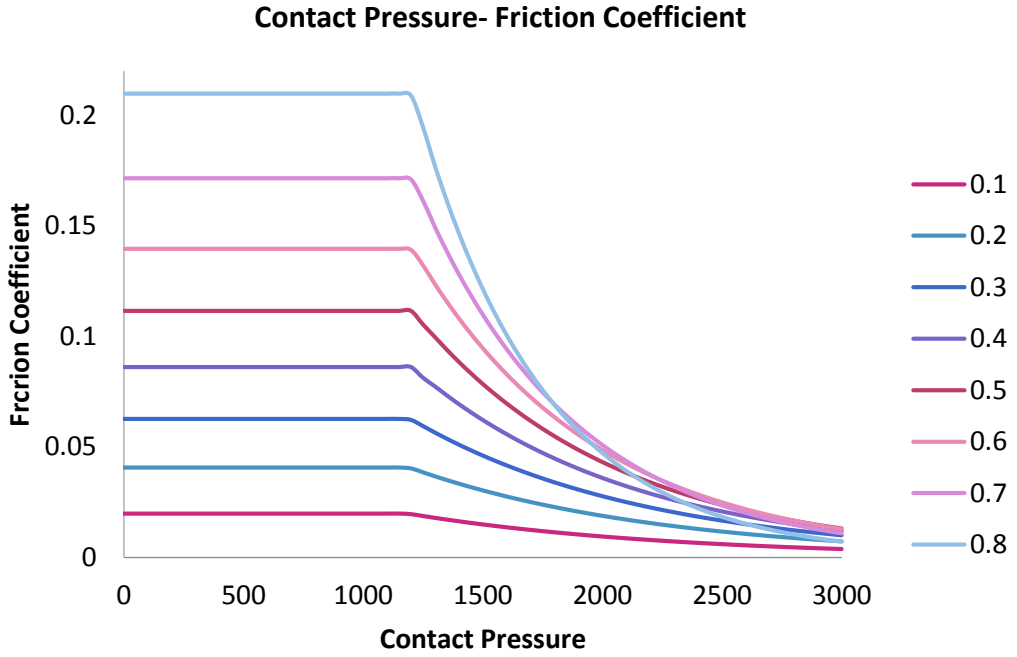

Figure 5.18 Calculated Friction Coefficient values for each contact pressure value

By using these curves, joining simulations have been performed. This model is integrated into ABAQUS. Experimental data, Coulomb Friction Model and Wanheim Bay Friction Model have been compared and results are shown in Figure 5.19.

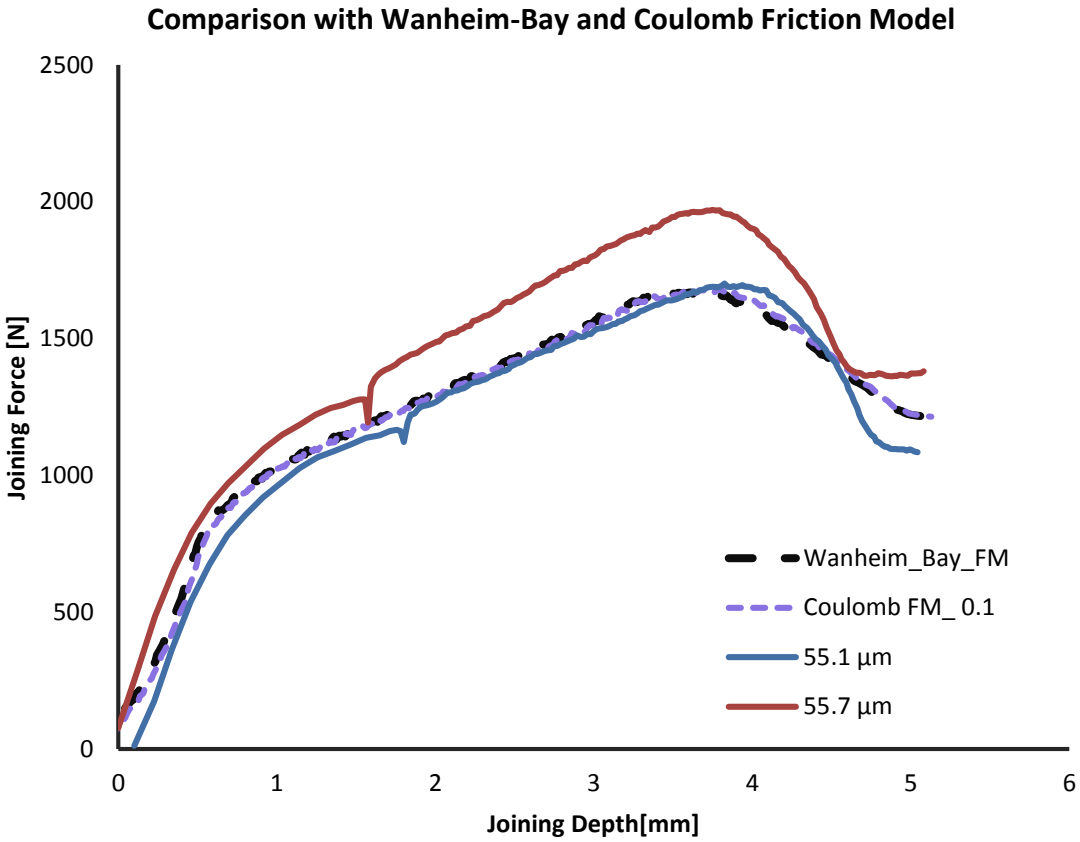

Figure 5.19 Comparison of Coulomb and Wanheim-Bay Friction Models

These study has been done by using actual process data. As shown in figure, the friction models are fitted well with the actual process. However, simple and grooved geometry trials are fitted 0.14 in Coulomb Friction model but in real process the coefficient is 0.1 for 55.1 µm results. As also can be seen in figure, the variance of the actual process data for same interference fit value is about %25. As mentioned before, the grooved geometry results have almost same difference. It is considered that, measurement of the filter could be caused the variance about the same interference value results. The results compared with the grooved geometry results. Following figure represents the comparison of these results.

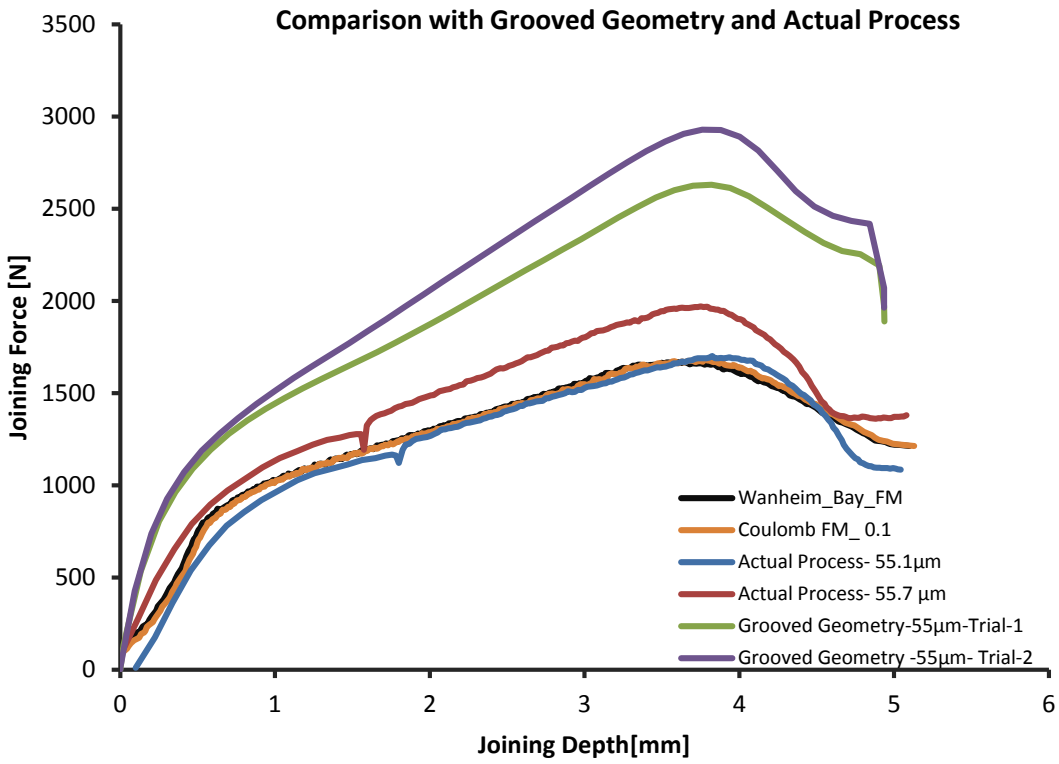

Figure 5.20 Comparison with Grooved Geometry and Actual Process in Same Overlap Value

In order to understand the difference about friction coefficient values, the grooved geometry and real process data are compared to each other. Grooved geometry has been designed by using actual process geometry. The difference between actual process and grooved geometry is;

- In actual geometry, the inside of the body, where the pin is settled, is coated with phosphate.
- The joining velocity is different each other. The experimental trials take 1 second while the actual process took 1.66 second.
- The other undefined parameters can affect the actual process. The centering pin into tube procedure is different to experimental process.

5.5 Studies of Analytical Model for Joining Process

In this study, joining process has been investigated experimental and numerical way. Also, process parameters have been examined by using these two methods. The system is investigated also analytical way by using DIN 7190 standards [22].

This standard specifies the basis of calculation for the interference fits with cylindrical effective surfaces, the parts of which consist of metallic materials. The assumptions of the process are;

- Uniform Deformation
- Elastic-plastic process
- Perfectly plastic in plastic region

Depending on the level of outer and inner parts as a result of a joining, a differentiation is made between pure elastic, elastic-plastic and full plastic interference fits. In elastic plastic interference fits, both elastic and plastic loaded ranges occur in inner and/or outer parts.

While designing interference fits, there are two calculation methods which are;

- Calculation method 1: Given joint pressure p, effective interference U_w and interference U are computed.
- Calculation method 2: Given interference U and effective interference U_w, joining pressure p is computed.

In both methods of calculation, it is first tested whether the predefined values lead to permissible loads in inner and outer parts. Finally, the required determinants are calculated. [22]

- In present standard, a simple calculation process, restricted in its scope of application, is specified for the elastic-plastically loaded interference fits; the use of this calculation method requires that the following pre-requisites must be fulfilled:

a) The inner part must be solid (Q_I=0)
b) Inner and the outer parts must have same elasticity constants. (E_I=E_A=E , μ_A=μ_B=μ=)

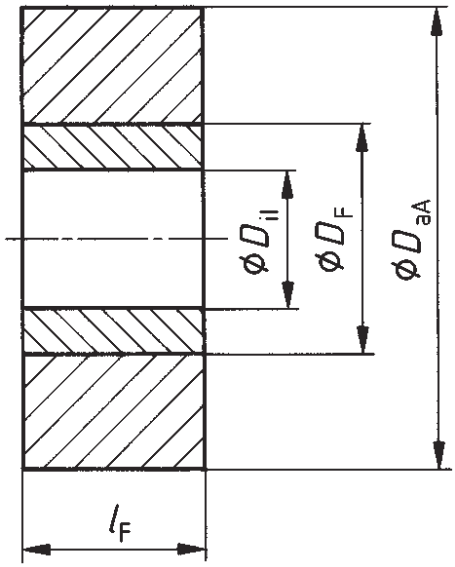

Figure 5.21 Calculation Model [22]

The calculation process of this standard is applicable to the interference fits with same constant axial length for inner and outer parts. Figure 6.17 shows the calculation model of the process. D_{il} refers inner diameter of the filter, D_{aA} refers outer diameter of the body and D_f represents diameter of the nominal joint.

The symbols and data which are used in calculations are shown in following chart;

Table 5.3 Explanation of symbols for analytical model

Symbol	Name	Unit
D_{iA}	Inner diameter of the outer part	mm
D_{aA}	Outer diameter of the outer part	mm
D_{aL}	Outer diameter of the inner part	mm
D_{iL}	Inner diameter of the inner part	mm
L_f	Length of the joint	mm
U_i	Actual interference	mm
D_f	Diameter of the joint	mm
U_w	Effective interference	mm

Symbol	Name	Unit
$Q_ı$	Diameter ratio of the inner	-
E_w	Reference effective interference	-
ζ_{ul}	permissible reference plasticity diameter of the outer part	-
P_{pi}	joining pressure limit for fully plastic inner part	N/mm^2
P_{pa}	joining pressure limit for fully plastic outer part	N/mm^2
R_{eLA}	lower yield stress of the outer part	N/mm^2
R_{eLI}	lower yield stress of the inner part	N/mm^2
E_A	elasticity modulus of the outer part	N/mm^2
E_I	elasticity modulus of the inner part	N/mm^2
μ_A	Poisson ratio of the outer part	-
μ_I	Poisson ratio of the inner part	-
R_{zA}	Average roughness depth of joint surface of the outer part	µm
R_{zI}	Average roughness depth of joint surface of the inner part	µm

To calculate the maximum forces in analytical method, calculations were made according to the specified flow diagram.

For the design of interference fits, the diameter ratios,

$Q_A = D_f/D_{aA}$ and $Q_ı = D_{il}/D_f = 0$ (because the inner part is solid)

The reference effective interference;

$E_w=U_w/D_f$ are required.

Eq.5.3

The effective interference U_w is calculated by using following formula;

$U_w= U-0.8(R_{zA}+R_{zL})$ Eq.5.4

The joining pressure limit p_{pA} for the fully plastic load of the outer part results from the equations;

If $Q_a <1/e$; p_{pA} is used to calculation.

$P_{pA} = \frac{2}{\sqrt{3}} R_{eLA}$ $Eq.5.5$

The relative plasticity diameter is determined by solving the transcendent equation;

$2\ln 3 - (Q_a.\zeta)^2 + 1 - \sqrt{3}\frac{P_{pA}}{R_{eLA}} = 0$ (Eq.5.6) and the reference plasticity diameter must satisfy the condition;

$$1\leq \zeta \leq \frac{1}{Q_a}$$

After ζ is calculated by iteratively, the reference effective interference E_w must lie within the range ;

$$\frac{2}{\sqrt{3}}\frac{R_{eLA}}{E} < E_w < \frac{2}{\sqrt{3}}\frac{R_{eLA}}{E}\zeta_{ul}{}^2$$

The relative effective plasticity diameter ζ of the outer part that results during the relative effective interference E_w is;

$\zeta = 0.931\frac{E_w.E}{R_{eLA}}$ $Eq.5.7$

Finally, the joining pressure is calculated by following method. And then force is calculated.

$$P = \frac{R_{eLA}}{\sqrt{3}}\left[1 + 2ln\zeta - \left(Q_A.\zeta\right)^2\right] \qquad Eq.5.8$$

After these calculations, experimental forces and analytical forces are compared to each other. These calculations are repeated each interference fit value. Interference fit value are determined by using experimental data.

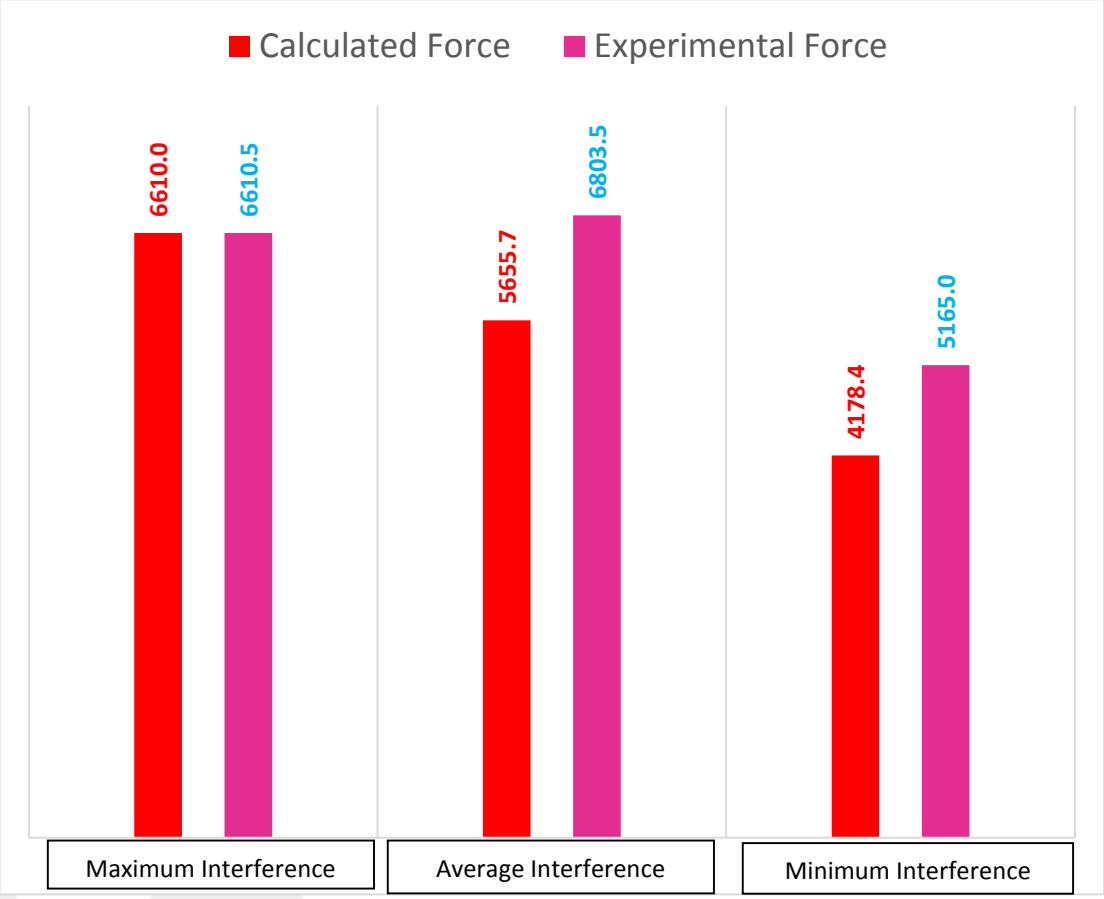

Figure 5.22 Comparison of Calculated vs Experimental Forces

As shown in this figure the error between two forces do not exceed 17 %. Maximum interference fit joint forces are almost same values.

Analytical model research and validation parts are still discussed to obtain more accurate solutions. Because in the all theoretical calculation parameters have been checked again and some parameter studies need to be repeated.

5.6 Studies to develop the actual process

When the process mechanics have been investigated, some parameters effects are examined by using numerical and experimental methods. To prevent dropping the

filter from injector, the holding force is need to be increased. For this reason, different parameters effects are investigated that how the holding force is affected.

- Tube Entrance Angle: As mentioned previous sections, when the tube entrance angle has been increased, the joint force is also increased.

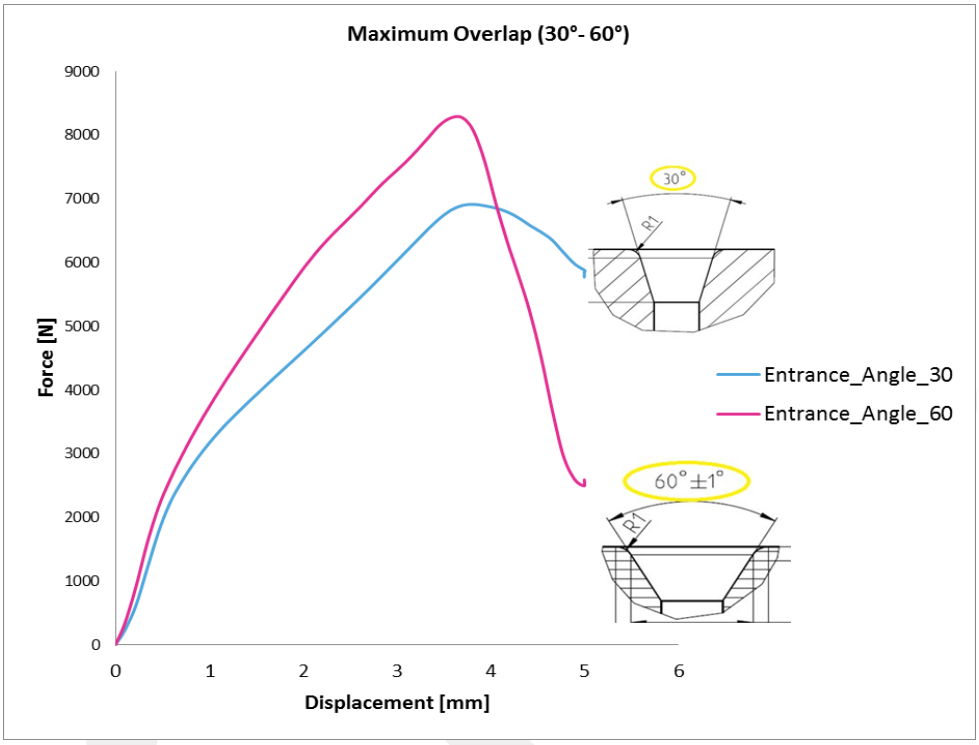

Figure 5.23 Comparison of the different entrance angle

When the angle value has been increased, the maximum force and joint strength change critically. While the tube entrance angle has been increased, the top of the filter which is wider than the tube entrance, pulled away so that the dimension of the filter decreases and the last joining force decreases.

- Pin Contact Area: Pin contact area affects the holding force because while the contact area is increasing, holding force also increases.

Pin contact area is extended for investigating this parameter effect. Two cases are examined. In theoretically, the contact area has been enhanced accordingly the maximum force has reached higher value.

- **Case 1:** Contact Area

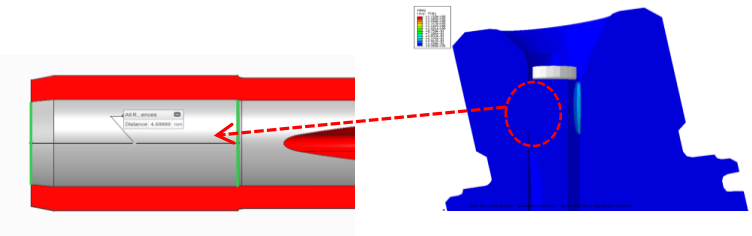

Figure 5.24 Contact Area of the Actual Geometry

- **Case 2:** Contact Area + %50

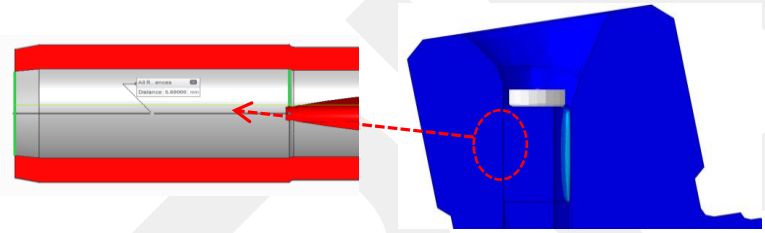

Figure 5.25 Situation of the Case 2

The aim of this study is to investigate and to prove that the holding area increases the holding force proportionally.

Figure 5.26 Comparison of Case 1 and Case 2

Analysis results show that, when the contact is increased, the holding force value reach to maximum. While the joining force is increased, the holding area of the filter and tube is going up higher. The main aim of this process, as mentioned before, is to increase holding area for reaching better fit.

CHAPTER 6

CONCLUSION

Increasing the complexity of product has driven the development of new joining process for mechanical parts especially in automotive industry. Joining by interference fits refer to joining of two components which are typically cylindrical shape. The fit is occurred by pressing the pin into a tube which creates a contact pressure at the interface. This contact pressure holds two parts together through friction, creating a mechanical joint [23].

This study focuses on analysis of elastic-plastic interference fit joints for three different geometry which are simple geometry, grooved and the geometry of actual process. The actual process is also joining of two mechanical parts, filter and tube, which are used in automotive injection system.

One of the aim of the study is to investigate process parameters of joining process in order to provide which parameters affect the system critically.

The studies of the joining process started with a brief problem definition, literature survey of the process. Next, a detailed parametrical studies have been done for three different geometries. These studies have been performed by using experimental, numerical and analytical methods.

To clear up affecting parameters, studies of boundary condition is performed. Effects are grouped under four main headings which are material properties, interference fit values, friction and geometrical properties of materials.

With this scope, firstly, a proper material characterization has been done for used materials which is essential for FEA (Finite Element Analysis) as the accuracy of outputs of simulation depends on the quality of the input material data. After that, joining trials have been done for examination of three separate geometries to make process more understandable.

For a more detailed analysis of the process, numerical methods are used to examine joining behavior. Numerical modelling studies have been done and these results

compare with the experimental results. The frictional behavior of the process has also been researched.

Finally, other process parameters which are geometrical properties of materials and studies to develop actual process were examined.

Analysis of the process has led to following conclusions;

- The most important output of these studies is to understand mechanics of process. Firstly, as the pin is pushed into tube, both pin and tube deform elastically at an early stage. At mid stage, tube is elastic, with the pin (filter) deforming plastically. At the late stage, as both pin and tube deforms plastically and the joining forces start to decrease. Secondly, maximum interference does not provide maximum joint strength; instead the joining force seems to reach the maximum around average interface value. Third, the force in the grooved geometry is approximately one half of the force for simple geometry, in direct proportion to the pin and tube contact area.
- Coulomb friction model agrees well with both simple and grooved geometry which is a coefficient value of 0.14. All interference value range has been examined by using both numerical and experimental methods and results compared with each other.
- In pin-tube geometry experiments gave almost same force-displacement curve however, grooved geometry has some changes of the force value. The main reason of this problem could be measurement of the filter geometry. The filter has grooves and it's hard to measure full-length dimensions properly. The difference of the same interference value curves is up to %15.
- When the friction model is applied to actual process, the coefficient value decrease to 0.1. Also, as mentioned before, the variance of actual process data existed. When this situation compared to grooved geometry, the unpredictable results have been obtained. The difference between actual and grooved geometry could be explained as follows;
    - In actual geometry, the inside of the body, where the pin is settled, is coating with phosphate.
    - The joining velocity is different each other. The experimental trials takes 1 second while the actual process took 1.66 second.

    - The other undefined parameters can affect the actual process. The centering pin into tube procedure is different to experimental process. Also, direction of the joining in actual process has specified angled.
- The process has also been investigated by using analytical method. The results showed that the analytical model needed to be improved.
- Lastly, it should be mentioned about the future work of the process. Following issues can be examined to get more detailed solution.
    - Surface quality of the parts
    - Coating effects
    - Material modification
    - Velocity of joining process
    - Lubrication
    - Also, the friction model also can be improved and Wanheim-Bay Friction model can be implemented to simple and grooved geometry results.

REFERENCES

[1] Ganesan V., Internal Combustion Engines, McGraw Hill Education (India) Pvt Ltd, 2012, p. 650

[2] Huyuk. H., Music O., Koç A., Karadoğan C., Bayram Ç., Analysis of Elastic Plastic Interference Fit Joints, ICTP, 2014

[3] Kim, S. S., Lee, D. G., Design of the hybrid composite journal bearing assembled by interference fit. Composite Structures, 2006, 75(1-4), 222–230.

[4] Croccolo, D., De Agostinis, M., & Vincenzi, N., How to improve static and fatigue strength in press-fitted joints using anaerobic adhesive. Proceedings of the Institution of Mechanical Engineers, 2011, Part C: Journal of Mechanical Engineering Science, 225(12), 2792–2803.

[5] Croccolo, D., Agostinis, M. D., & Vincenzi, N., Design of hybrid steel-composite interference fitted and adhesively bonded connections, 2012, International Journal of Adhesion and Adhesives, 37, 19-25.

[6] Lewis, R., Measurement of interface pressure in interference fits. Proceedings of the Institution of Mechanical Engineers, 2005, Part C: Journal of Mechanical Engineering Science, 219(2), 127–139.

[7] Kawamura H, Sawa T, Yoneno M, Nakamura T Effect of fitted position on stress distribution and strength of a bonded shrink fitted joint subjected to torsion, 2003.

[8] Yang, G. M., Coquille, J. C., Fontaine, J. F., & Lambertin, M., Influence of roughness on characteristics of tight interference fit of a shaft and a hub, 2001, International Journal of Solids and Structures, 38(42-43), 7691-7701.

[9] Zhang, Y., McClain, B., & Fang, X., Design of interference fits via finite element method, 2000, International Journal of Mechanical Sciences, 42(9), 1835–1850.

[10] Lippmann, H., The effect of a temperature cycle on the stress distribution in a shrink fit, 1992, International Journal of Plasticity, (1), 567–582.

[11] O. Eyercioglu, M. A. Kutuk, N. F. Yilmaz, Shrink fit design for precision gear forging dies, Journal of Materials Processing Technology, 209 (2009), 2186-2194

[12] Yoneno M, et al. Sealing performance of liquid sealant in flexible box-shape flange bolted joints, ASME Pressure Vessels Piping Conference, vol. PVP 354. New York: ASME; 1997. p. 179–84

[13] Wang, G. S., Stress analysis for a lug under various condition, 1994, The Journal of Strain Analysis for Engineering Design, 29(1), 7–16.

[14] T. N. Chakherlou, M. Mirzajanzadeh, J. Vogwell, B. Abazadeh, 2011, Investigation of the fatigue life and crack growth in torque tightened bolted joints, Aerospace Science and Technology 15(4)(2011) 304–313.

[15] T. N. Chakherlou, M. Mirzajanzadeh, Kh. Saeedi, Fatigue crack growth behavior and life prediction of a single interference fitted holed plate, 2010, Fatigue Fracture Engineering Materials and Structures 33(10)(2010) 633–644

[16] Behrens, Bernd-Arno; Bouguecha, Anas; Hadifi, Tarik, Advanced friction modeling for bulk metal forming processes, 2011.

[17] Xincai Tan, Comparisons of the Friction Models in Bulk Metal Forming, 2002, Tribology International, v.35, pp. 385-393

[18] S.B. Petersen, P.A.F. Martins, Bay N., Friction in Bulk Metal Forming: A General Friction Model vs. The law of Constant Friction, 1995.

[19] Wanheim, T., Friction at High Normal Pressures, 1973.

[20] T. Wanheim, Bay N., Petersen A.S., A Theoretically Determined Model for Friction in Metal Working Process, 1973.

[21] ABAQUS User Manual, version 6.13.4

[22] DIN Standard 7190:2001-02

[23] Mori, K., Bay, N., Fratini, L., Micari, F., Tekkaya, A.E., Joining by plastic deformation, 2013, CIRP Annals - Manufacturing Technology, 62(2), 673-694.